International Journal of Hydrogen Energy 234 (2026) 154957

Contents lists available at ScienceDirect

International Journal of Hydrogen Energy

journal homepage: www.elsevier.com/locate/he

# Environmental Potential Of Co-Transporting Hydrogen In Natural Gas Pipelines Followed By Electrochemical Hydrogen Compression

Karan Anand [a], Georgia Ioanna Prokopou [b], Wibke Zängler [c], Vu Phong Nguyen [d], Hendrik Pötting [a], Robert Keller [c], Alexander Mitsos [b,e,f], Matthias Wessling [c,g], Niklas von der Assen [a,*]

[a] RWTH Aachen University, Institute of Technical Thermodynamics, Schinkelstr. 8, 52062, Aachen, Germany
[b] RWTH Aachen University, Process Systems Engineering, Forckenbeckstr. 51, 52074, Aachen, Germany
[c] RWTH Aachen University, Chemical Process Engineering, Forckenbeckstr. 51, 52074, Aachen, Germany
[d] TLK Energy GmbH, Heinrichsallee 41, 52062, Aachen, Germany
[e] JARA-ENERGY, 52056, Aachen, Germany
[f] Institute of Climate and Energy Systems, Energy Systems Engineering (ICE-1), Forschungszentrum Jülich GmbH, 52425, Jülich, Germany
[g] DWI - Leibniz Institute for Interactive Materials, RWTH Aachen University, 52074, Aachen, Germany

ARTICLE INFO

*Keywords:*
Electrochemical hydrogen compression
Hydrogen separation
Hydrogen supply chain
Life cycle assessment
Hydrogen and natural gas co-transport

ABSTRACT

Green hydrogen ($H_2$) produced via water electrolysis and renewable electricity is promising to defossilize energy-intensive sectors. Options to deliver $H_2$ to consumers include $H_2$ pipelines as well as co-transport in existing natural gas (NG) pipelines. $H_2$/NG co-transport requires subsequent separation and compression, as $H_2$ consumers require high-purity $H_2$ at elevated pressures. Electrochemical Hydrogen Compression (EHC) is an emerging technology for both separation and compression. We conduct a cradle-to-gate Life Cycle Assessment of $H_2$/NG co-transport in NG pipelines with EHC. We compare $H_2$/NG co-transport with EHC against co-transport with Pressure Swing Adsorption, pure $H_2$ pipelines, and fossil $H_2$, among others, with respect to 16 environmental impact categories. $H_2$/NG co-transport with EHC can achieve similar greenhouse gas (GHG) emissions as pure $H_2$ pipelines, and can reduce GHG emissions by up to 91% compared to fossil $H_2$ if the supply chain is powered by wind electricity. However, if the GWI of electricity exceeds ~260 $g_{CO2\text{-}eq}/kWh_{el}$, all green $H_2$ transport routes have higher GHG emissions than fossil $H_2$. Furthermore, these GHG emission reductions are accompanied by increased environmental impacts in at least 9 categories.

## 1. Introduction

The mitigation of climate change requires the defossilization of energy-intensive sectors, such as chemicals, steel and mobility. In many cases, direct electrification using renewable electricity sources (RES) is a viable option [1,2]. However, direct electrification poses challenges for some energy-intensive sectors because they require energy carriers with high gravimetric energy densities [3]. One promising energy carrier is green hydrogen ($H_2$), produced via water electrolysis and renewable electricity [4]. Since green $H_2$ is often not produced where it is consumed, an infrastructure is needed to transport $H_2$ [5]. One of the main challenges for storage and transport is hydrogen's low volumetric density [6].

Pipelines are considered a promising $H_2$ transport option due to low emissions compared to other options [7]. The infrastructure for pipelines exists in many countries for transport of natural gas (NG) [8], e.g., 500,000 km in Germany [9,10]. The existing NG pipeline infrastructure can be retrofitted to either co-transport $H_2$ with NG, or to transport $H_2$ in dedicated pure $H_2$ pipelines [11,12]. Consequently, both pure $H_2$ pipelines and co-transport in NG pipelines are part of $H_2$ distribution strategies of some countries, such as Australia [13] and Germany [9,10].

Co-transporting $H_2$ in NG pipelines requires subsequent separation and compression of $H_2$ since most $H_2$ consumers, e.g., $H_2$ refueling stations, require high-purity $H_2$ at elevated pressures [14,15]. Pressure Swing Adsorption (PSA) is a well-established technology for $H_2$ separation from high-concentration feeds in industrial processes such as Steam Methane Reforming (SMR) [16]. However, PSA has not been used for separating $H_2$ from feeds with relatively low concentrations of $H_2$,

* Corresponding author.
*E-mail address:* niklas.vonderassen@ltt.rwth-aachen.de (N. von der Assen).

https://doi.org/10.1016/j.ijhydene.2026.154957
Received 16 January 2026; Received in revised form 13 March 2026; Accepted 8 April 2026
Available online 21 April 2026
0360-3199/© 2026 The Authors. Published by Elsevier Ltd on behalf of Hydrogen Energy Publications LLC. This is an open access article under the CC BY license (http://creativecommons.org/licenses/by/4.0/).

such as up to 20 vol.-% in $H_2$/NG co-transport [16–20]. Furthermore, additional mechanical compressors are needed in PSA systems, which can be energy-intensive [17]. A promising emerging alternative is Electrochemical Hydrogen Compression (EHC), which can both separate and compress $H_2$ in a single device [18,21]. Theoretically, EHC has the potential to achieve purities greater than 99.97 % [18] at up to 900 bar [22] with $H_2$ recovery rates up to 100 % [20]. Currently, practical challenges such as high energy demands up to 16 $kWh/kg_{H2}$ [15] due to high ohmic losses and back-diffusion of $H_2$ lower the overall performance of EHC [20,23].

For $H_2$/NG co-transport including subsequent separation and compression via EHC to be a viable transport option, its economic feasibility and environmental impacts should be favorable over those of $H_2$/NG co-transport with PSA as well as alternative pure $H_2$ transport routes. While economic feasibility drives technology adoption, green $H_2$ is deployed to meet environmental sustainability targets, and therefore the environmental impacts of $H_2$/NG co-transport with EHC need to be comparable to or lower than those of alternative $H_2$ supply routes. However, these environmental impacts have not been comprehensively assessed, making it unclear whether $H_2$/NG co-transport with EHC can enable $H_2$ supply at low environmental impacts.

Neacsa et al. [24] calculated the Global Warming Impact (GWI) of combusting $H_2$/NG mixtures, while Cappello et al. [25] and Di Lullo et al. [26] determined the GWI during transport and combustion of $H_2$/NG mixtures. Davis et al. [27] assessed the GWI mitigation potential and cost effectiveness of $H_2$/NG mixtures across an economy. Bellocchi et al. [28] determined the environmental impacts of $H_2$/NG mixtures across multiple scenarios, while considering blended end-use. None of the mentioned studies considered the subsequent separation and compression of $H_2$ from NG and in particular, none assessed EHC as an alternative separation and compression technology from an environmental perspective. Further, the mentioned studies did not compare the environmental impacts of $H_2$ supply via NG pipelines to other $H_2$ transport routes. Aminov et al. [29] compared $H_2$/NG co-transport to other $H_2$ transport routes from an economic perspective while considering membranes for $H_2$ separation. Di Lullo et al. [30] compared the greenhouse gas (GHG) emissions of $H_2$/NG co-transport to other $H_2$ transport routes while considering PSA for $H_2$ separation. The study demonstrated that the lowest costs and GHG emissions are achieved through $H_2$/NG co-transport and pure $H_2$ pipelines [30].

In summary, studies assessing the environmental impacts of $H_2$/NG co-transport remain limited. In particular, no study determined the environmental impacts of $H_2$ separation and compression via EHC. Thus, the environmental potential of $H_2$/NG co-transport with subsequent separation and compression via EHC, as well as its comparison to alternative $H_2$ supply routes, remains an open research gap.

Our study closes the identified research gaps by conducting a cradle-to-gate Life Cycle Assessment (LCA) of $H_2$ separation and compression via EHC, as well as $H_2$/NG co-transport in NG pipelines with EHC to enable $H_2$ supply. For $H_2$ separation, we include PSA as alternative technology in our assessment. We further compare the environmental impacts of $H_2$/NG co-transport to other promising $H_2$ transport options, i.e., transport in new pure $H_2$ pipelines, transport of liquid $H_2$ in fuel-cell electric trucks, and the transport of electricity with $H_2$ production at consumer-site. Fossil $H_2$ from SMR serves as benchmark. We also assess the risk of environmental burden-shift by evaluating 16 environmental impact categories, as recommended by the Joint Research Center (JRC) of the European Commission [31]. Furthermore, we perform in-depth parameter variations covering various pipeline assumptions, mixture conditions, transport distances and GHG emissions for the electricity used in the supply chain to obtain potential environmental trade-offs with other $H_2$ transport options. Ultimately, the aim of this study is to assess the environmental potential of supplying $H_2$ through the existing NG infrastructure using EHC.

## 2. Life Cycle Assessment (LCA)

The environmental assessment is conducted through an LCA as defined in the ISO 14040/44 standards [32]. An LCA study is conducted in four steps: 1) Goal and scope definition, 2) Life Cycle Inventory (LCI), 3) Life Cycle Impact Assessment (LCIA) and 4) Interpretation [32].

### 2.1. Goal & scope definition

The goal of this study is to assess the cradle-to-gate environmental impacts of co-transporting green hydrogen ($H_2$) and natural gas (NG) in existing NG pipelines with subsequent $H_2$ separation and compression via Electrochemical Hydrogen Compression (EHC). The environmental impacts of $H_2$/NG co-transport with EHC are compared to other promising $H_2$ transport options. To ensure a consistent comparison across all transport options, all environmental impacts are expressed relative to the so-called Functional Unit (FU). The FU is defined as "1 kg *high-purity hydrogen at end pressure* $p_{end}$" for all $H_2$ supply options.

$H_2$ end pressure levels $p_{end}$ of 16 bar (only separation), 100 bar, 300 bar and 700 bar are considered to examine how EHC performs for different compression ratios. The end pressure levels of 100 bar and 300 bar are representative for requirements from industrial consumers [33], whereas 700 bar is the pressure level for $H_2$ refueling stations [34]. Furthermore, various volume percentages of $H_2$ during $H_2$/NG co-transport are considered, i.e., $x_{H2} = 5$, 10, 15, 20 and 50 vol.-%. Since EHC is not a mature technology yet, a base and optimistic case are modeled: The base case corresponds to operating conditions, which are reachable in the near future, whereas the optimistic case reflects target conditions for future development.

Fig. 1 gives an overview of the $H_2$/NG co-transport routes. In all co-transport routes, it is assumed that the $H_2$/NG mixture is transported from the production to the consumer site via a primary pipeline at operating pressure $p_{op}$. Afterwards, $H_2$ is separated from NG with one of the following two separation technologies: EHC and Pressure Swing Adsorption (PSA). While EHC includes compression of separated $H_2$ in a single device, PSA requires subsequent mechanical compression. We assume a $H_2$ purity after separation of at least 99.97 %, making it suitable for $H_2$ refueling stations [35].

The NG stream after the separation unit still contains a fraction of $H_2$ due to incomplete recovery. The NG stream including unrecovered $H_2$ is fed into a secondary pipeline at the operating pressure $p_{sec}$. Depending on the separation unit and the pressure of the secondary pipeline $p_{sec}$, further compression of the unrecovered stream might be required, which can result in increased energy demands [30].

When $H_2$ and NG are co-transported, a fraction of the pipeline capacity is used to transport $H_2$. We distinguish between two cases how this fraction of the pipeline capacity was used before transporting $H_2$:

1. **No excess capacity:** All available NG pipelines are fully used to transport NG. The fraction of the pipeline capacity now used to transport $H_2$ was previously used to transport NG. Hence, $H_2$ replaces NG which needs to be transported otherwise to still ensure that the NG demand is satisfied. We assume that a new pipeline segment needs to be built to transport the replaced NG, and corresponding environmental impacts from pipeline construction are considered.
2. **Excess capacity:** In this case, a fraction of the pipeline capacity is unused due to gradual phase-out of NG to reach defossilization targets. This unused pipeline capacity is now used to co-transport $H_2$ with NG. No new pipeline needs to be built.

For the comparison of the two separation and compression technologies (EHC vs. PSA incl. mechanical compression), we first consider a gate-to-gate system boundary for separation and compression of $H_2$ from the $H_2$/NG mixture (see Fig. 2). This narrow system boundary allows to understand the detailed energy demands and gate-to-gate GHG emissions.

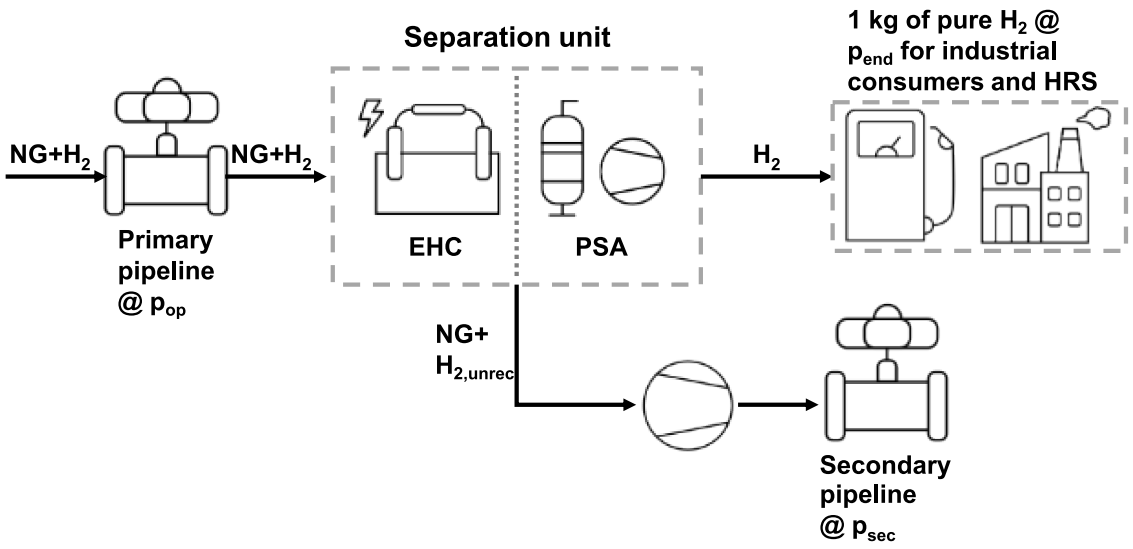



**Fig. 1.** Overview of hydrogen ($H_2$) and natural gas (NG) co-transport including the separation unit and $H_2$ consumer. The $H_2$/NG mixture is transported in the primary pipeline, which operates at operating pressure $p_{op}$. Then, the separation unit separates $H_2$ from the $H_2$/NG mixture such that the desired $H_2$ product at the desired end pressure level $p_{end}$ exits the separation unit. As basis for comparison, we define a Functional Unit of 1 kg of high-purity $H_2$ at $p_{end}$. Since the separation units have incomplete $H_2$ recovery, the unrecovered $H_2$, together with the NG builds the unrecovered $H_2$/NG mixture, which is fed into a secondary pipeline operating at $p_{sec}$. EHC: Electrochemical Hydrogen Compression, PSA: Pressure Swing Adsorption including subsequent mechanical compression.

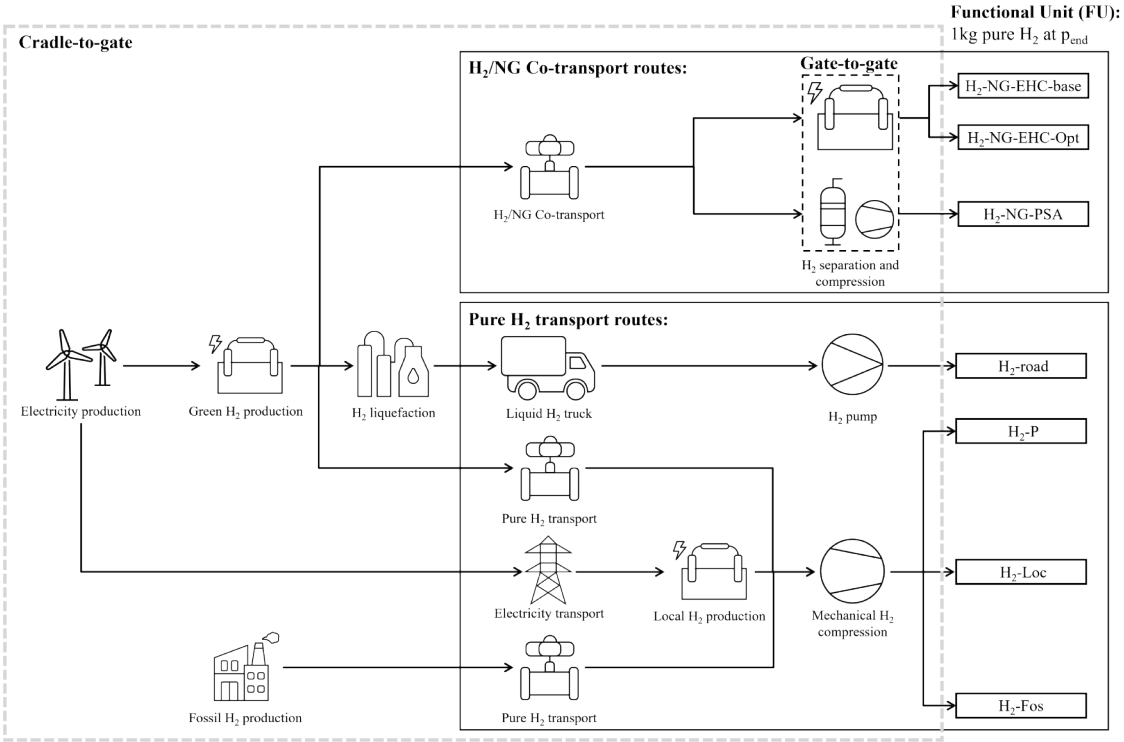



**Fig. 2.** Cradle-to-gate system boundary of the hydrogen ($H_2$) supply options. $H_2$-NG-EHC-base and $H_2$-NG-EHC-opt are transport routes where $H_2$ is co-transported in natural gas (NG) pipelines and then separated via Electrochemical Hydrogen Compression (EHC). Base and opt refer to the base and optimistic case of the EHC. $H_2$-NG-PSA describes $H_2$/NG co-transport with subsequent $H_2$ separation via Pressure Swing Adsorption (PSA). For the $H_2$/NG co-transport routes, we also define an alternative gate-to-gate system boundary to compare the two technologies for separation and compression. $H_2$–P describes $H_2$ transport in new pure $H_2$ pipelines, $H_2$-Road describes the transport of liquid $H_2$ in fuel-cell electric trucks and $H_2$-Loc describes the transport of electricity with subsequent decentralized $H_2$ production at the consumer site. $H_2$-Fos is the fossil benchmark where $H_2$ is produced via Steam Methane Reforming (SMR) and transported via $H_2$ pipelines. SMR: Steam Methane Reforming. $p_{end}$: End pressure of final $H_2$ product.

Since this study aims to assess several $H_2$ supply options, a second system boundary is chosen considering cradle-to-gate (see Fig. 2), which includes $H_2$ production and transport but excludes the use-phase and end-of-life. This study primarily assesses the environmental impacts of $H_2$/NG co-transport with EHC. To assess the environmental potential of EHC, a base model of EHC (**$H_2$-NG-EHC-base**) and an optimistic model

of EHC (**$H_2$-NG-EHC-opt**) are considered. As alternative technology for $H_2$ separation, PSA is included (**$H_2$-NG-PSA**). To evaluate whether $H_2$/NG co-transport is a promising option for $H_2$ supply, its environmental impacts are compared to four pure $H_2$ transport routes (see Fig. 2). These include green $H_2$ transport in new pure $H_2$ pipelines (**$H_2$–P**), transport of liquid $H_2$ via fuel cell electric-trucks (**$H_2$-Road**), transport of electricity, the decentral local production of green $H_2$ at the consumer-site (**$H_2$-Loc**) and the fossil production of $H_2$ via SMR and transport via $H_2$ pipelines (**$H_2$-Fos**).

As default, this study assumes a fixed transport distance of 1000 km and wind electricity from a representative wind farm in Northern Germany (see Section 2.1 in Supporting Information for details) as electricity source in the entire supply chain. This setup roughly represents transporting the renewable electricity from Northern Germany via $H_2$ to Southern Germany. Pure wind electricity as power supply is a best-case assumption, leading to the lowest possible impacts. For an electricity supply that is fully based on wind electricity, the environmental impacts are higher, as further components, such as storages are required for a reliable electricity supply [36].

An overview of all the considered parameter variations is given in Table 1.

**Table 1**
Overview of all considered parameter variations. $H_2$: Hydrogen, NG: natural gas, $x_{H2}$: Volume percentage of $H_2$ in $H_2$/NG mixture, $p_{end}$: End pressure of final $H_2$ product, $p_{op}$: Operating pressure of primary pipeline (see Fig. 1), $p_{sec}$: Operating pressure of secondary pipeline (see Fig. 1), Note a: Only separation.

| Parameter | Type | Range/ Values | Relevance | Default Value(s) |
|---|---|---|---|---|
| End pressure of $H_2$ $p_{end}$ | Discrete | 16[a], 100, 300 and 700 bar | 100 and 300 bar are representative for industrial consumers, while 700 bar is representative for $H_2$ refueling stations. | 16 and 700 bar |
| Volume percentage of $H_2$ in $H_2$/NG mixture $x_{H2}$ | Discrete | 5, 10, 15, 20, 50 vol.-% | Up to 20 vol.-% possible today in German gas grids [37]. 50 vol.-% included as future reference. | 20 vol.-% |
| Transport distance | Continuous | 0-5000 km | Captures environmental trade-offs for varying transport distances. | 1000 km |
| Global Warming Impact of electricity source in the supply chain | Continuous | 0-450 $g_{CO2}$/$kWh_{el}$ | Captures environmental trade-offs for various electricity impacts | Wind electricity (15 $g_{CO2}$/$kWh_{el}$, see Section 1.1 in SI) |
| Excess capacity | Discrete | Yes and no | Defines whether the fraction of the existing pipeline capacity used to transport $H_2$ during $H_2$/NG co-transport was previously utilized for pure NG transport or was available as excess capacity (see Section 2.1 and 2.2.4). | Yes |
| EHC model | Discrete | Base and Optimistic model (compare Section 2.2.8) | Included to reflect development targets as the EHC is not a mature technology yet | Both models included in transport routes (see Fig. 2) |
| Operating pressure of secondary pipeline $p_{sec}$ | Discrete | 1 and 16 bar | Injection of the unrecovered $H_2$/NG mixture of the separation unit into mid- (1 bar) or high-pressure (16 bar) distribution pipelines. | $p_{sec}$ = 16 bar |
| Operating pressure of primary pipeline $p_{op}$ | Discrete | 16 and 100 bar | Transport of the $H_2$/NG mixture or pure $H_2$ in high-pressure distribution (16 bar) or long-distance transport pipelines (100 bar). | $p_{op}$ = 16 bar |

## 2.2. Life Cycle Inventory

The Life Cycle Inventory (LCI) comprises a foreground and background system. The foreground system consists of all modeled processes such as $H_2$ production and transport, while the background system covers all supporting processes such as raw material supply. All background processes are modeled using ecoinvent v3.9.1 [38]. In the following, the main parts of the foreground system are described, while a detailed overview of the data used can be found in the Supporting Information (SI).

### 2.2.1. Hydrogen production

Green $H_2$ production is modeled via Proton Exchange Membrane (PEM) electrolysis, where water is split into $H_2$ and oxygen using renewable electricity. An energetic efficiency of 70 % is assumed, based on literature data [39–42]. For the materials consumed in the construction of the electrolyzer, the near-future inventory from Bareiβ et al. [40] and Sharma et al. [41] is adopted. As a benchmark, fossil $H_2$ production via SMR, based on the LCI from Antonini et al. [43] is assumed. The full LCI data for fossil and green $H_2$ production can be found in Table 6-10 of the SI.

### 2.2.2. Hydrogen liquefaction

Liquefying $H_2$ is energy-intensive and a current field of research. The specific energy consumption ranges from 6 to 15 $kWh/kg_{H2}$ [44–46], and thus, the average of 10.5 $kWh/kg_{H2}$ is assumed. The construction of the liquefaction plant is modeled using the LCI data from Stolzenburg and Mubbala [47] with a plant lifetime of 30 years and a production capacity of 50 $t_{H2}$/d. The full LCI data can be found in Table 13 of the SI.

### 2.2.3. Mechanical hydrogen compression

For the construction of the $H_2$ compressor, the LCI data provided by Kanz et al. [48] for a 12 MW piston compressor with a lifetime of 50 years is assumed. As stated by Tahan [49], 0.5 % of $H_2$ is assumed to be lost during compression. The energy demands and the nominal power are calculated according to Khan et al. [50] (see Section 1.2 in the SI). The supply chain requires $H_2$ compressors in the pipelines, after the pipelines and between the electrolyzer and the pipelines. For the different compressor powers, the LCI from Kanz et al. [48] is scaled linearly. The full LCI data can be found in Tables 11 and 12 of the SI.

### 2.2.4. Pipeline transport

$H_2$ can be transported through existing NG pipelines with varying volume percentages of $H_2$. The $H_2$/NG mixture in the pipeline is modeled as an ideal gas mixture. As $H_2$ and NG are co-transported, the joint environmental impacts of co-transport need to be allocated to $H_2$ individually. To allocate the environmental impacts of $H_2$/NG co-transport, a consequential approach is applied.

In the consequential approach, the additional environmental impacts of co-transport of $H_2$ relative to transporting only NG are quantified. Through mixing $H_2$ with NG, the leakage rate, recompression energy and required maintenance during transport increase for the $H_2$/NG mixture compared to pure NG. These additional environmental impacts are attributed to $H_2$ transport during $H_2$/NG co-transport.

Furthermore, it is distinguished between two cases depending on how the fraction of the pipeline capacity was used prior to transporting $H_2$ during $H_2$/NG co-transport (see Fig. 3). In the *no excess capacity* case, it is assumed that the fraction of the pipeline capacity, which transports $H_2$ during $H_2$/NG co-transport was previously used to transport NG. Since the total NG supply to end users should remain constant even upon co-transporting $H_2$ with NG, a new pipeline segment needs to be built to transport that portion of NG that is replaced by $H_2$. The environmental impacts of constructing the new pipeline segment are included in our assessment (see Fig. 3 and Section 2.4 of the SI). In contrast, in the *excess capacity* case, it is assumed that the part of the pipeline capacity used to transport $H_2$ was previously unused due to ongoing defossilization and thus declining NG demand. In this case, the unused pipeline capacity transports $H_2$, while the NG demand is still fulfilled during $H_2$/NG co-transport. Consequently, no additional infrastructure is required, and only the aforementioned increased operational impacts resulting from $H_2$/NG co-transport are considered.

In addition to the consequential approach, an energy-based allocation of infrastructure impacts is analyzed in Section 2.4 of the SI. Both approaches yield similar results for all considered scenarios (see Fig. S8 in Section 3.2 of the SI), as the operational impacts are identical in both approaches and only the allocation of pipeline construction impacts differs.

The construction of new $H_2$ pipelines is modeled by accounting for the required amount of steel and the $H_2$ flow rate, in accordance to two technical reports of the JRC [38,51,52]. The lifetime of the new $H_2$ and $H_2$/NG co-transport pipelines is assumed to be 40 years, as modeled in the ecoinvent dataset for NG pipelines [38].

The leakage rate for $H_2$ in the co-transported pipelines is assumed to be the same as in the pure $H_2$ pipelines, i.e., 0.5 % per 1000 km [48]. For $H_2$/NG co-transport, this leakage rate represents a conservative upper bound for the $H_2$-attributable leakage. The leakage rate of a $H_2$/NG mixture is lower than that of pure $H_2$ due to the lower leakage rate of NG. Thus, only the $H_2$ fraction of the leaked gas would be attributed to $H_2$ transport, resulting in a lower bound for $H_2$ losses in the co-transported pipeline. However, the higher diffusivity of $H_2$ leads to preferential leakage through seals, enriching the leaked gas in $H_2$ relative to the $H_2$/NG composition in the co-transported pipeline. The real $H_2$-attributable leakage therefore lies between the allocated mixture leakage and the pure $H_2$ leakage rate assumed in our study. Additionally, it is accounted for an increase in pipeline maintenance equivalent to 2% of the natural gas pipeline's construction impacts due to the co-transport of $H_2$ [53,54]. For the pure $H_2$ pipelines, a 2% maintenance factor is applied to the $H_2$ pipeline construction [48,54,55].

Furthermore, for the pure $H_2$ transport and $H_2$/NG co-transport, the transport in two primary pipelines with different operating pressures $p_{op}$ are considered (see Table 1). Recompression stations are required every 100 km along the $H_2$ pipelines to maintain operation. For the distribution pipelines, the compression from 11 to 16 bar requires 0.179 kWh/(100 km · $kg_{H2}$) [50]. The full LCI data for $H_2$/NG co-transport can be found in Tables 14–34, while the full LCI data for pure $H_2$ pipeline transport can be found in Tables 35–36 of the SI.

### 2.2.5. *Electricity transport*

Alternatively, to supply $H_2$, electricity could be transported in high-voltage alternating current (HVAC) transmission lines with the decentral production of $H_2$ at the consumer-site. The environmental impacts during the construction of the HVAC transmission lines are included in this study. The produced electricity from wind turbines is at high voltage, thus it is assumed that no additional transformers are needed.

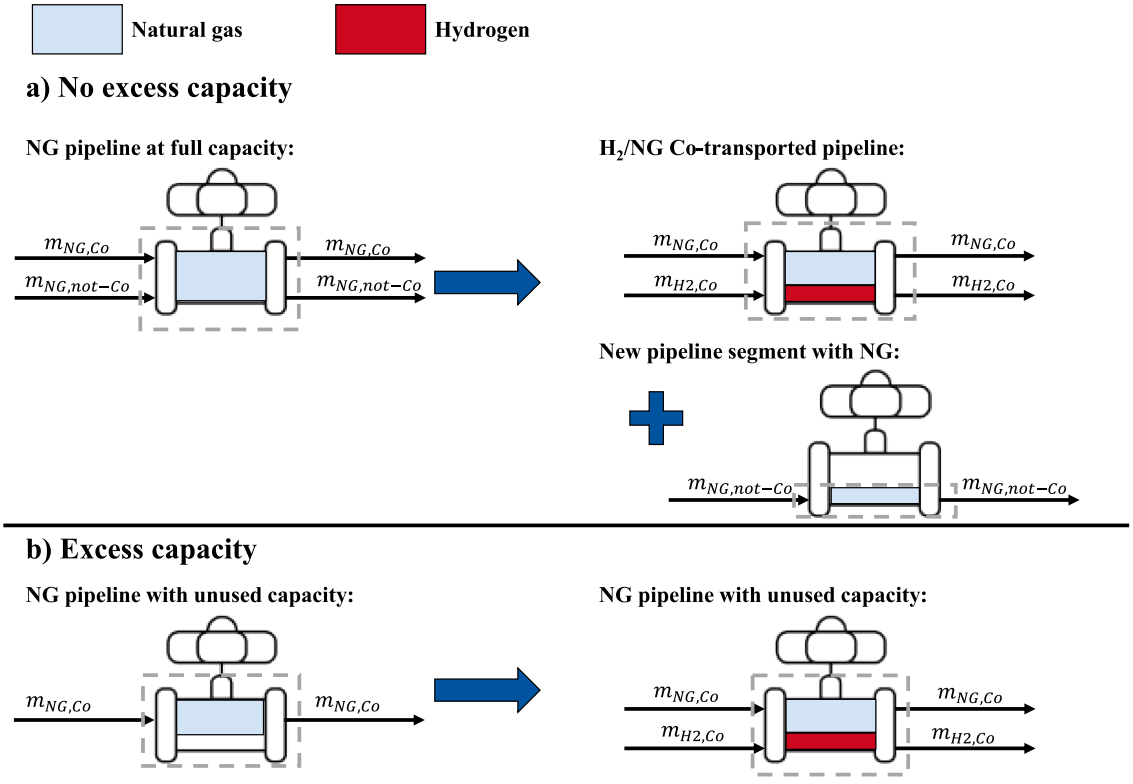



**Fig. 3.** System boundaries of hydrogen ($H_2$) and natural gas (NG) Co-transport in the a) No excess capacity and b) Excess capacity case. $m_{NG,not-Co}$: NG mass transported in the fraction of the pipeline capacity used to transport $H_2$ in the $H_2$/NG co-transported pipeline, $m_{NG,Co}$: NG mass transported with $H_2$ in the $H_2$/NG co-transported pipeline, $m_{H2,Co}$: $H_2$ mass transported during $H_2$/NG co-transport.

Losses of 1 %/100 km are assumed for the transmission [56]. The full LCI data is given in Table 37 of the SI.

### 2.2.6. Road transport

We choose 40 ton fuel-cell electric trucks for transporting the liquid $H_2$ via road. To model the truck construction, the LCI for fuel-cell electric trucks from Sacchi et al. [57] is modified such that the trucks transport liquid $H_2$ instead of compressed $H_2$ to achieve higher volumetric densities. To model the liquid $H_2$ tank, a ratio of 14.56 $kg_{tank}/kg_{LH2}$ with the corresponding material demands from Weiszflog et al. [58] is assumed. The trucks have a lifespan of 710,000 km and an average load factor of 29 % [57]. The boil-off is assumed to be 0.1 %/d [58], while the trucks have an average truck speed of 80 km/h, with the truck travelling 800 km daily [57]. The full LCI data is given in Table 38 of the SI.

### 2.2.7. Hydrogen regasification & pumping

In contrast to the liquefaction of $H_2$, the regasification requires limited effort. Liquid $H_2$ is usually heated with ambient air or seawater, which results in exergy losses [59]. While technical options for recovering this exergy exist, they are not yet implemented [59]. Prior to heating, a cryopump pumps $H_2$ to the desired end pressure $p_{end}$, which reduces the energy demand compared to compressing gaseous $H_2$ [46,59]. $H_2$ losses of 0.5 % are assumed [49] and for the construction, the same nominal power and LCI as for the $H_2$ compressors is assumed. The full LCI data is given in Table 39 of the SI.

### 2.2.8. Hydrogen separation

For the $H_2$/NG co-transport routes (see Fig. 1), the inlet pressure for both separation units is 16 bar, which corresponds to the outlet pressure of the high-pressure distribution pipeline. We assume that the secondary pipeline can either be a high- or mid-pressure distribution pipeline. The mid-pressure distribution pipeline has an inlet pressure of 1 bar. For both separation units, it is assumed that 0.1 % of the $H_2$ is lost during the process for handling $H_2$ [52].

*2.2.8.1. Electrochemical hydrogen compression.* EHC consists of electrochemical cells, where $H_2$ and NG enter a flow-channel at the anode. Upon applying a voltage to the EHC, $H_2$ reacts to H+ ions and electrons at the anode, whereas NG is inert in the reaction at anode (see Fig. 4). The H+ ions migrate through the membrane to the cathode, where they recombine to molecular $H_2$ leading to a product stream with high $H_2$ concentration. Through pressurization of the cathode, the $H_2$ product has high pressures. Theoretically, high efficiencies at high pressures are reachable with EHC, however, cell irreversibilities, such as ohmic losses and $H_2$ back diffusion due to pressure gradients between cathode and anode lower the efficiencies in practice [14,18].

The overall energy demand of EHC consists of an electric energy demand needed for the electrochemical reactions, membrane and the theoretical minimum work of separation, of a heating demand required to heat the gases to stack temperature, and of a cooling demand to maintain the stack temperature [14,60]. The energy demands are obtained from a 1D simulation model in Modelica using the Software Dymola 2023x and the model library Hydrogen Energy Systems 3.14.0 (see Section 1.3 of SI). Due to the low maturity of EHC, a base case, which corresponds to near-future conditions and an optimistic case, which refers to future target conditions, is modeled. In the base case, voltage and faradaic efficiencies are calculated within the simulation model, accounting for ohmic, activation and $H_2$ back-diffusion losses. In both the base and optimistic case, EHC operates at a cell temperature of 40 °C with a cell area of 50 $cm^2$. The base case represents the simulation data of EHC with an operating current density of 1 $A/cm^2$ with $H_2$ recovery rates between 68 and 80 %. The optimistic case assumes that higher current densities of 2 $A/cm^2$ with recovery rates between 90 and 98 % can be reached, depending on the volume percentage of $H_2$ in the $H_2$/NG mixture [61] (see Table 2 and Section 1.3 of SI for details).

In the base case, it is assumed that the low-temperature heating demand above 40 °C is covered through a water-air heat pump powered by grid electricity. For the cooling demand, the use of cooling water from an unspecified natural origin is assumed, which is modeled as biosphere flow.

Since ohmic resistances dominate the voltage losses, a membrane with higher conductivity is assumed in the optimistic case leading to lower ohmic resistance (see Section 1.3 of SI). Additionally, the faradaic efficiency is set to 100 % in the optimistic case, assuming that no $H_2$ back-diffusion or incomplete reactions occur. The heating and cooling

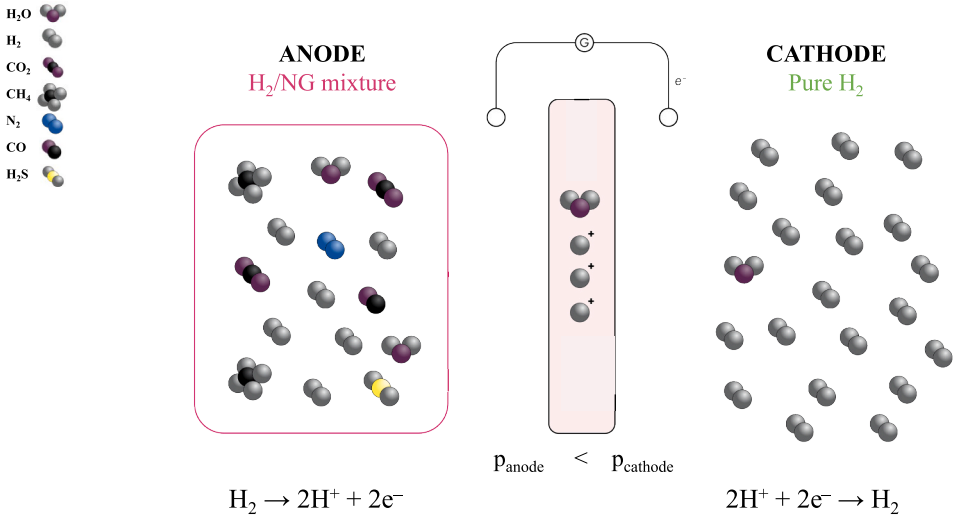



**Fig. 4.** Operation principle of Electrochemical Hydrogen Compression (EHC), adapted from Ref. [18]. The $H_2$/NG mixture is fed to the anode, where $H_2$ reacts to H+ ions. The H+ ions migrate through the proton-conducting membrane, while the components in NG are blocked. At the pressurized cathode, H+ ions recombine with electrons to form pure and compressed $H_2$. $H_2$: Hydrogen, NG: Natural gas, $H_2O$: Water, $CO_2$: Carbon dioxide, $CH_4$: Methane, $N_2$: Nitrogen, CO: Carbon monoxide, $H_2S$: Hydrogen sulfide, $p_{cathode}$: Cathode pressure, $p_{anode}$: Anode pressure.

**Table 2**
Main LCI data for Electrochemical Hydrogen Compression (EHC) with a feed gas containing 20 vol.-% $H_2$ for different $H_2$ end pressure levels $p_{end}$. The data for the other volume percentages are summarized in the SI. $w_{el,EHC}$: Electric energy demand of EHC, $w_{th,EHC}$: Heating demand of EHC, $w_{cool,EHC}$: Cooling demand of EHC. $H_2$: Hydrogen.

| Parameter | | Base | Optimistic | Sources |
|---|---|---|---|---|
| Lifetime [a] | | 7 | 10 | [40,41] |
| Current density $\left[\frac{A}{cm^2}\right]$ | | 1 | 2 | own assumption |
| $H_2$ recovery rate [%] | | 68.5 | 92 | own assumption, based on [61] |
| Only Separation | $w_{el,EHC}$ $\left[\frac{kWh}{kg_{H2}}\right]$ | 11.38 | 6.24 | Values obtained from 1D simulation model. In optimistic case, the model is adapted for novel membrane material and no faradaic losses (see Section 1.3 in SI). |
| | $w_{th,EHC}$ $\left[\frac{kWh}{kg_{H2}}\right]$ | 1.69 | 1.69 | Values obtained from 1D simulation model |
| | $w_{cool,EHC}$ $\left[\frac{kWh}{kg_{H2}}\right]$ | 12.05 | 12.05 | Values obtained from 1D simulation model |
| 100 bar | $w_{el,EHC}$ $\left[\frac{kWh}{kg_{H2}}\right]$ | 12.18 | 6.9 | Values obtained from 1D simulation model. In optimistic case, the model is adapted for novel membrane material and no faradaic losses (see Section 1.3 in SI). |
| | $w_{th,EHC}$ $\left[\frac{kWh}{kg_{H2}}\right]$ | 1.53 | 1.53 | Values obtained from 1D simulation model |
| | $w_{cool,EHC}$ $\left[\frac{kWh}{kg_{H2}}\right]$ | 12.56 | 12.56 | Values obtained from 1D simulation model |
| 300 bar | $w_{el,EHC}$ $\left[\frac{kWh}{kg_{H2}}\right]$ | 12.73 | 7.29 | Values obtained from 1D simulation model. In optimistic case, the model is adapted for novel membrane material and no faradaic losses (see Section 1.3 in SI). |
| | $w_{th,EHC}$ $\left[\frac{kWh}{kg_{H2}}\right]$ | 1.44 | 1.44 | Values obtained from 1D simulation model |
| | $w_{cool,EHC}$ $\left[\frac{kWh}{kg_{H2}}\right]$ | 13.12 | 13.12 | Values obtained from 1D simulation model |
| 700 bar | $w_{el,EHC}$ $\left[\frac{kWh}{kg_{H2}}\right]$ | 13.38 | 7.6 | Values obtained from 1D simulation model. In optimistic case, the model is adapted for novel membrane material and no faradaic losses (see Section 1.3 in SI). |
| | $w_{th,EHC}$ $\left[\frac{kWh}{kg_{H2}}\right]$ | 1.47 | 1.47 | Values obtained from 1D simulation model |
| | $w_{cool,EHC}$ $\left[\frac{kWh}{kg_{H2}}\right]$ | 13.77 | 13.77 | Values obtained from 1D simulation model |

demands are assumed to be the same as in the base case. However, the heating demand is covered by available waste heat, thereby assuming no additional environmental burdens for heat supply. The cooling demand is met with cooling water, modeled the same as in the base case.

For the material demands of the EHC, the same materials as for a PEM electrolyzer are assumed with the only exception that the anode catalyst is platinum for EHC instead of iridium for PEM. The same inventory as Sharma et al. [41] and Bareiβ al. [40] is assumed as they provide a base and optimistic case for the material demands of the PEM electrolyzer. The LCI data is summarized in Table 2Table 40-Table 45 of the SI of the SI.

*2.2.8.2. Pressure Swing Adsorption.* PSA is an established technology for $H_2$ separation from reforming gases and is currently used in the chemical and petroleum refining industry [17,62]. Typically, the feed consists of high volumetric concentration of $H_2$ (>70 vol.-%) [16], thus using PSA for the separation of $H_2$ from NG at low concentrations is not conventional. In the PSA, methane and other heavy gases in NG are adsorbed in the column so that a purified $H_2$ stream passes through the column. In this work, a PSA process in accordance to Dehdari et al. [16] is assumed, which consists of six columns and twelve steps in each cycle. A higher number of columns is necessary to facilitate the pressure equalization steps, which increase the $H_2$ recovery for lower $H_2$ concentrations in the feed stream [16].

The choice of the adsorbents in the PSA system are crucial for the operational performance. In accordance to Dehdari et al. [63], a pre-layer of silica gel to adsorb heavy hydrocarbons and $CO_2$, activated carbon to adsorb methane and zeolite in a post-layer to adsorb nitrogen is chosen.

One challenge for PSA systems is to maximize both $H_2$ recovery and purity [16,63,64]. Typically, PSA can achieve $H_2$ purities in the range of 98–99.999 %, with a $H_2$ recovery rate between 70 and 90 % [64,65], with recent work suggesting high recoveries of >80% for high purity $H_2$ (>99%) [16]. The recovery rates are taken from Dehdari et al. [16], who provide recovery rates for 5-30 vol.-% $H_2$. However, two adjustments are made: First, it is assumed that the purity requirements for fuel cells of >99.97 % are met in each case and second, since the authors do not provide values for 50 vol.-%, it is assumed that the recovery rate achieved for 30 vol.-% $H_2$ can also be achieved for 50 vol.-%.

The energy demand for the PSA includes the compression of the $H_2$ product stream to the desired end pressure $p_{end}$ and of the unrecovered $H_2$/NG mixture to the operating pressure of the secondary pipeline $p_{sec}$ (see Fig. 1). Since the desorption pressure of the PSA is 1 bar, the unrecovered $H_2$/NG mixture could be directly fed into a mid-pressure distribution pipeline operating at $p_{sec} = 1$ bar. Otherwise, if the unrecovered $H_2$/NG mixture is fed back into the high-pressure distribution pipeline with $p_{sec} = 16$ bar, the unrecovered mixture stream needs to be compressed as well, leading to higher energy demands (see Section 1.2 of SI). Both cases for the unrecovered $H_2$/NG mixture are considered in this analysis.

For the construction of the PSA, the demand of stainless steel for the valves and columns and the material demands of the adsorbents are included. All material demands for the PSA system are taken from Dehdari et al. [63]. Selected LCI parameters for the PSA are summarized in Table 3, while the full LCI data can be found in Table 51 of the SI.

### 2.3. Life Cycle Impact Assessment

We use Environmental Footprint (EF) v3.1 [31] to translate the biosphere flows into environmental impacts. As recommended by the Joint Research Center (JRC) of the European Commission, we include 16 different environmental impact categories in our analysis to assess the risk of environmental burden-shifting [31]. However, according to EF v3.1, the *GWP100* characterization factor of $H_2$ is 0, whereas recent studies show that $H_2$ could form methane or other greenhouse gases in the atmosphere and is therefore also associated with a characterization factor [66]. Studies show that the characterization factor of $H_2$ for *GWP100* ranges from 5 to 12 [66–69]. We follow the results of Sand et al. and assume a *GWP100* characterization factor of 11.6 for $H_2$ [66].

## 3. Results

This section is divided into three subsections. In the first subsection, we focus on detailed analyses of the environmental impacts of $H_2$ separation and compression (see Fig. 2). In the second subsection, we compare the cradle-to-gate environmental impacts of $H_2$/NG co-transport with subsequent $H_2$ separation and compression to the alternative pure $H_2$ transport routes (see Fig. 2). In the third subsection, we discuss our findings.

### 3.1. Analysis of hydrogen separation and compression

In Section 3.1.1, we analyze the electricity demand and Global Warming Impact (GWI) of $H_2$ separation and compression via EHC and PSA, but without considering the other supply chain steps (gate-to-gate system boundary in Fig. 2). In Section 3.1.2, we analyze the cradle-to-gate GWI of $H_2$/NG co-transport with $H_2$ separation and compression for various volume percentages of $H_2$ in the $H_2$/NG mixture.

#### 3.1.1. Electricity demand and Global Warming Impact of hydrogen separation and compression

For 20 vol.-% $H_2$, the base model of EHC consumes 11.4-13.4 kWh/$kg_{H2}$ (see Fig. 5a). Changing the membrane material such that EHC has lower ohmic and $H_2$ back-diffusion losses (see Section 1.3 of SI) halves the electricity demand in the optimistic case compared to the base case. The electricity demand of PSA depends on the pipeline into which the unrecovered $H_2$ and NG are fed. If the unrecovered $H_2$/NG mixture remains at the desorption pressure of 1 bar, the unrecovered $H_2$/NG mixture can be fed into a mid-pressure distribution pipeline without additional compression. In this case, both the base and optimistic model of EHC consume more electricity than PSA (see Fig. 5a, $p_{sec} = 1$ bar). On the other hand, if the unrecovered $H_2$/NG mixture is fed into a high-pressure distribution pipeline, the unrecovered $H_2$/NG mixture needs to be compressed from 1 to 16 bar. In this case, electricity demand of the PSA ranges from 7.2 to 9.6 kWh/$kg_{H2}$ and is higher than the optimistic model of EHC (see Fig. 5a, $p_{sec} = 16$ bar). For EHC, no compression of the unrecovered $H_2$/NG mixture is needed as it exits EHC at inlet pressure, i.e., 16 bar.

To validate our results, we compare our modeled EHC energy demands to literature. For $H_2$ compression with atmospheric inlet pressure, Lipp achieves energy demands of 3-12 kWh/$kg_{H2}$ for compression up to 207 bar and 20 kWh/$kg_{H2}$ for compression up to 81.6 MPa [14,70]. Prokopou et al. [21] report energy demands of 11.7–17.2 kWh/$kg_{H2}$ for compression to 10–700 bar at 1 A/$cm^2$. For $H_2$ separation, Jackson et al. [71] report 3.5–12.5 kWh/$kg_{H2}$ at 0.2 A/$cm^2$, while Nordio et al. [72] report 3.72 kWh/$kg_{H2}$ for $H_2$ separation at 6 bar inlet pressure. Mrusek et al. [60] determine a thermal energy demand of 5.6–7.0 kWh/$kg_{H2}$ for gas heating and humidification, consistent with the heating demands in our model (see Table 5 of SI). Our base model has an electricity demand of 11.4–13.4 kWh/$kg_{H2}$, which is comparable with these studies. Lower energy demands in our study compared to Prokopou et al. [21] mainly result from the higher inlet pressure in our system, which reduces the compression ratio. Our optimistic model (5.7–8.1 kWh/$kg_{H2}$) is comparable to Dale et al., who report an energy demand of 7.5 kWh/$kg_{H2}$ for compression up to 138 bar [73]. The assumed improved membrane properties in our optimistic EHC model are supported by experimental demonstrations of Giner ELX Inc. who used a modified membrane with low $H_2$ back-diffusion to achieve an energy consumption of 2.0 kWh/$kg_{H2}$ at 350 bar end pressure [14,74].

For 20 vol.-% $H_2$, the gate-to-gate GWI of EHC-opt ranges from 0.1 to 0.12 $kg_{CO2\text{-}eq}$/$kg_{H2}$, which is lower than that of the PSA (0.13-0.21 $kg_{CO2\text{-}eq}$/$kg_{H2}$) for all considered end pressures if the unrecovered $H_2$/NG mixture is compressed to 16 bar (see Fig. 5b). If the unrecovered $H_2$/NG mixture remains at 1 bar, EHC-opt has a higher GWI than PSA (0.03-0.11 $kg_{CO2\text{-}eq}$/$kg_{H2}$) for all considered end pressures. The GWI of EHC-base ranges from 0.29 to 0.31 $kg_{CO2\text{-}eq}$/$kg_{H2}$, which is higher than that of PSA in all end pressure cases because of the high energy demand during separation and compression. For only separation ($p_{end} = 16$ bar), the material impacts of EHC-base are twice as high as those of PSA. For higher compression ratios, the material impacts of EHC-base and PSA are similar because the PSA system requires an additional compressor for the $H_2$ product, which is not needed in the case of only separation.

For lower volume percentages of $H_2$ in the $H_2$/NG mixture and $p_{sec} = 16$ bar (see Fig. S3 in SI), the amount of NG in the unrecovered $H_2$/NG mixture of PSA increases, leading to an increased electricity demand for compression (32.7-35.1 kWh/$kg_{H2}$ for 5 vol.-% $H_2$ and 16.4-18.8 kWh/$kg_{H2}$ for 10 vol.-% $H_2$) and an increased GWI (0.47-0.55 $kg_{CO2\text{-}eq}$/$kg_{H2}$ for 5 vol.-% $H_2$ and 0.25-0.33 kWh/$kg_{H2}$ for 10 vol.-% $H_2$). Consequently, for 5 and 10 vol.-% $H_2$, the GWI of both EHC-base (0.43-0.45 $kg_{CO2\text{-}eq}$/$kg_{H2}$ for 5 vol.-% $H_2$ and 0.33-0.35 kWh/$kg_{H2}$ for 10 vol.-% $H_2$) and EHC-opt (0.11-0.13 $kg_{CO2\text{-}eq}$/$kg_{H2}$ for 5 vol.-% $H_2$ and 0.1-0.12 kWh/$kg_{H2}$ for 10 vol.-% $H_2$) is lower or comparable to that of PSA.

#### 3.1.2. Global Warming Impact of hydrogen and natural gas co-transport including hydrogen separation and compression

In Fig. 6, we depict the cradle-to-gate GWI for $H_2$/NG co-transport with subsequent separation via PSA and EHC, including $H_2$ production; using different volume percentages of $H_2$ in the $H_2$/NG mixture and default values for variable parameters (see Table 1). The results for the long distance ($p_{op} = 100$ bar) yield similar results as high-pressure distribution pipelines ($p_{op} = 16$ bar) and are therefore included in Fig. S4 of the SI.

With increasing volume percentage $x_{H2}$ of $H_2$, the cradle-to-gate GWI

**Table 3**
Main LCI data for Pressure Swing Adsorption with a feed gas containing 20 vol.-% $H_2$ for $H_2$ end pressure levels $p_{end}$. $H_2$: Hydrogen. $p_{sec}$: Pressure level of the unrecovered $H_2$ and natural gas mixture (see Fig. 1).

| Parameter [unit] | Value | | Sources |
|---|---|---|---|
| Lifetime [a] | 40 | | [63] |
| $H_2$ recovery rate [%] | 80.84 | | [16] |
| **Parameter [unit]** | $p_{sec} = 1$ bar | $p_{sec} = 16$ bar | |
| Lifetime [a] | 40 | 40 | [63] |
| $H_2$ recovery rate [%] | 80.84 | 80.84 | [16] |
| $w_{el}\left[\frac{kWh}{kg_{H2}}\right]$, only separation | 0 | 7.22 | [50] |
| $w_{el}\left[\frac{kWh}{kg_{H2}}\right]$, 100 bar | 0.975 | 8.195 | [50] |
| $w_{el}\left[\frac{kWh}{kg_{H2}}\right]$, 300 bar | 1.63 | 8.85 | [50] |
| $w_{el}\left[\frac{kWh}{kg_{H2}}\right]$, 700 bar | 2.39 | 9.61 | [50] |

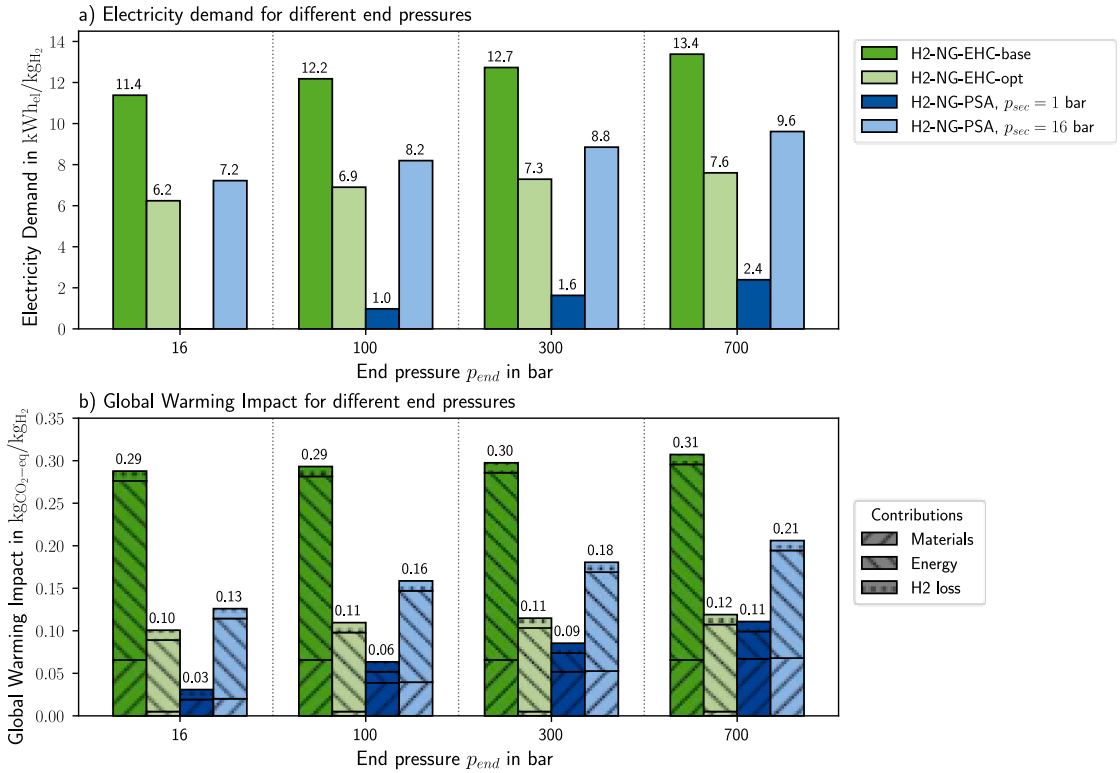



**Fig. 5.** Overview of the gate-to-gate electricity demands and Global Warming Impact (GWI) for separation and compression via the Electrochemical Hydrogen Compression (EHC) and Pressure Swing Adsorption (PSA) combined with mechanical compression. The transport distance is 0 km. The volume percentage of $H_2$ $x_{H2}$ is 20 vol.-%. $p_{sec}$: Pressure level of the unrecovered hydrogen and natural gas mixture (see Fig. 1). $p_{end}$: End pressure of the $H_2$ product. In $H_2$-NG-EHC-base and $H_2$-NG-EHC-opt, $H_2$ is separated via EHC. Base and opt refer to the base and optimistic case of EHC. In $H_2$-NG-PSA, $H_2$ is separated via PSA. $H_2$: Hydrogen.

decreases in all cases (see Fig. 6). The decreasing GWI with increasing volume percentage $x_{H2}$ for $H_2$/NG co-transport with EHC-base is caused by decreasing electricity and heating demands. For $H_2$/NG co-transport with EHC-opt, the changes in the GWI are minor as the heating demands are met through available waste heat. As discussed in Section 3.1.1, a lower volume percentage $x_{H2}$ increases the GWI of the PSA if the unrecovered $H_2$/NG mixture is compressed to 16 bar. $H_2$/NG co-transport with EHC-opt has a lower or similar GWI as PSA for all considered cases. EHC-opt is more favorable than PSA for $H_2$ separation and compression to 700 bar ($p_{end} = 700$ bar) than for only separation ($p_{end} =$ 16 bar), as the PSA operates at 16 bar and no additional mechanical compressor is required for the $H_2$ product. EHC can separate and compress $H_2$ in one device, making it more favorable for higher compression ratios.

Furthermore, we distinguish whether the portion of the existing pipeline used to transport $H_2$ during $H_2$/NG co-transport was previously utilized for pure NG transport or was available as excess capacity (see Section 2.1 and 2.2.4). An excess capacity in the original NG pipeline results in lower GWI due to lower construction impacts, while the overall trend in the GWI across the considered separation technologies and $H_2$ volume percentages remains consistent in both cases (see Fig. S4 of the SI).

While $H_2$/NG co-transport with PSA can achieve low GWI under ideal conditions ($p_{sec} = 1$ bar), this setup assumes that the unrecovered $H_2$/NG mixture does not require recompression, which is typically incompatible with pipeline injection requirements of higher pressures for safe and efficient $H_2$ transport. As a result, the recompression of the unrecovered $H_2$/NG mixture of the PSA is necessary ($p_{sec} = 16$ bar), increasing electricity demand and GWI, particularly at low $H_2$ volume percentages. In contrast, EHC offers greater flexibility: It can achieve low GWI at all $H_2$ volume percentages $x_{H2}$ and it can operate at high inlet pressures, eliminating the need for additional compression of the unrecovered $H_2$/NG mixture. While both EHC and PSA show competitive GWI for $H_2$ separation and compression, EHC offers greater integration flexibility into existing pipeline systems and has the potential of achieving lower GWI than the PSA system (see Figs. 5 and Fig. 6).

### 3.2. Comparison of hydrogen and natural gas co-transport to other hydrogen transport routes

In this subsection, we compare $H_2$/NG co-transport with EHC to the alternative pure $H_2$ transport routes (see Fig. 2). We first present a contribution analysis of the GWI in Section 3.2.1, followed by an analysis of environmental burden-shift in Section 3.2.2. In Section 3.2.3, we conduct a sensitivity analysis of the GWI for the electricity in the supply chain and the transport distance.

#### 3.2.1. Contribution analysis

$H_2$/NG co-transport with EHC has the potential to achieve a GWI that is lower than or equal to all other $H_2$ transport routes despite the additional energy-intensive separation and compression of $H_2$ (see Fig. 7).

If only separation is considered ($p_{end} = 16$ bar), all $H_2$/NG co-transport routes have higher impacts from separation and compression than pure $H_2$ transport routes as these do not require additional separation. Thus, if $p_{end} = 16$ bar, pure $H_2$ pipelines have the lowest GWI, followed by $H_2$/NG co-transport with EHC-opt (see Fig. 7a). If separation and compression to 700 bar is considered ($p_{end} = 700$ bar), $H_2$/NG co-transport with EHC-base or PSA have higher impacts from separation and compression than pure $H_2$ transport routes. For $H_2$/NG co-transport with EHC-opt, these impacts are comparable or even lower than in the pure $H_2$ transport routes due to improvements in material usage and energetic efficiency of EHC. Thus, for $p_{end} = 700$ bar, $H_2$/NG co-transport with EHC-opt has the lowest GWI, followed by pure $H_2$

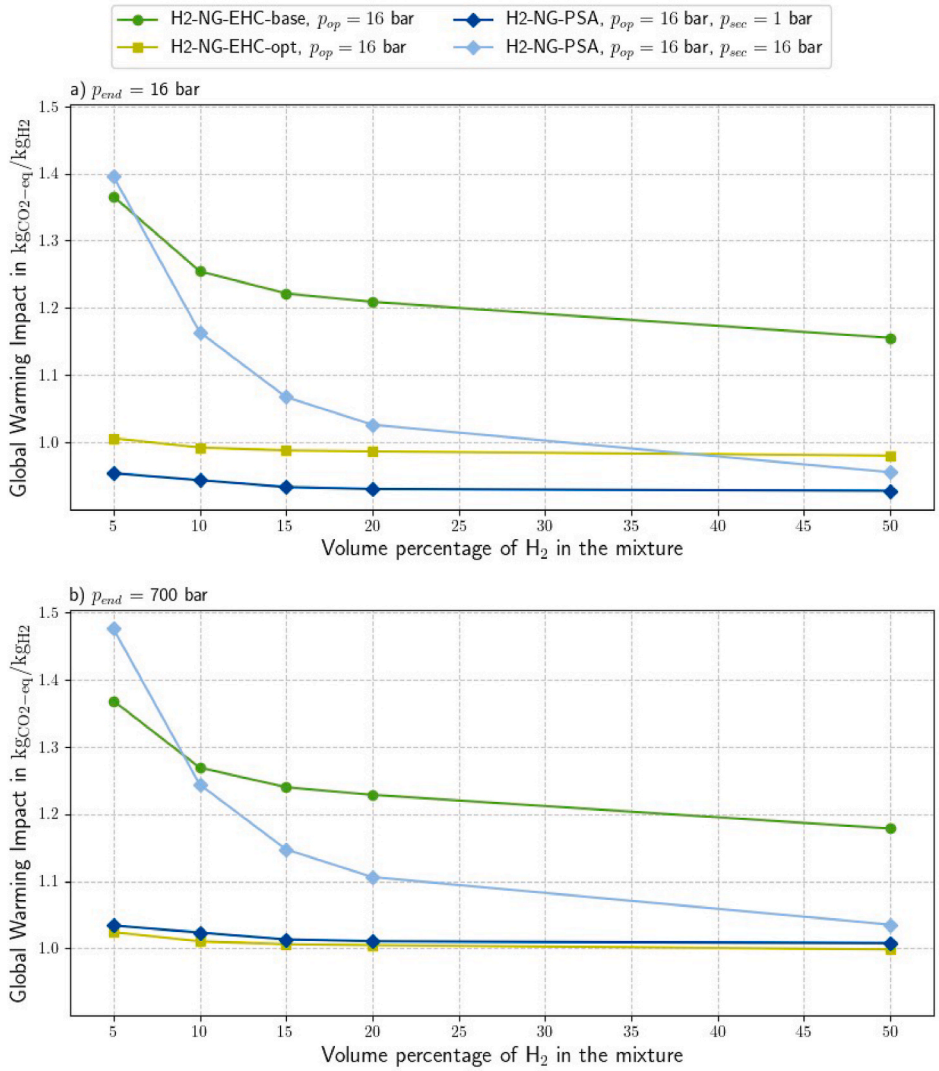



**Fig. 6.** Sensitivity analysis of the Global Warming Impact (GWI) with respect to the volume percentage of hydrogen ($H_2$) $x_{H2}$. The transport distance is 1000 km. We assume that the fraction of the pipeline capacity used to transport $H_2$ during $H_2$/NG co-transport was previously unused and available as excess capacity (see Table 1). $p_{sec}$ : Operating pressure of the secondary pipeline (see Fig. 1). $p_{op}$: Operating pressure of the primary pipeline (see Fig. 1). $p_{end}$: Final pressure of the $H_2$ product. The subplot a) shows only separation at 16 bar, whereas the subplot b) shows the case of separation and compression to 700 bar. $H_2$-NG-EHC-base and $H_2$-NG-EHC-opt are transport routes where $H_2$ is co-transported with natural gas (NG) in NG pipelines and then separated via Electrochemical Hydrogen Compression (EHC). Base and opt refer to the base and optimistic case of the EHC. In $H_2$-NG-PSA, $H_2$ is co-transported with NG but subsequently separated via Pressure Swing Adsorption (PSA).

pipelines (see Fig. 7b). In both end pressure cases, the GWI of $H_2$/NG co-transport with EHC-opt is lower than that with PSA. $H_2$/NG co-transport with EHC-base has a higher GWI than with PSA but similar GWI as local $H_2$ production and a lower GWI than transport of liquid $H_2$ via trucks.

If the original NG pipeline had an excess capacity for $H_2$ co-transport, the infrastructure impacts are lower than for pure hydrogen pipelines because no new pipeline segment is necessary. If the existing NG pipeline had no excess capacity for $H_2$ co-transport, a new pipeline segment needs to be built to transport the amount of NG that is replaced by $H_2$. In this case, the infrastructure impacts of $H_2$/NG co-transport and pure hydrogen pipelines are comparable, and the ranking between these routes depends primarily on the separation and compression impacts. Under both assumptions, $H_2$/NG co-transport with EHC-opt has a lower GWI than pure $H_2$ pipelines at $p_{end} = 700$ bar. At $p_{end} = 16$ bar, pure $H_2$ pipelines have a lower GWI than $H_2$/NG co-transport under both assumptions, as no additional separation and compression is required for pure $H_2$ pipelines. For EHC-base, the excess capacity assumption can change the ranking relative to electricity transport and local $H_2$ production ($H_2$-Loc): without excess capacity, EHC-base has a higher GWI than $H_2$-Loc at $p_{end} = 16$ bar, while at $p_{end} = 700$ bar, EHC-base has a lower GWI. With excess capacity, EHC-base achieves a lower GWI than $H_2$-Loc at both end pressures (see Fig. 7).

To validate our LCA results, we compare our results to published values for known $H_2$ transport routes. For pure $H_2$ pipeline transport, Wulf et al. [55] determine a GWI of 1.5–1.7 $kg_{CO2\text{-}eq}/kg_{H2}$ at 700 bar end pressure over distances up to 400 km, Akhtar et al. [7] obtain 1.57 $kg_{CO2\text{-}eq}/kg_{H2}$ for a 300 km pipeline and 700 bar end pressure, and De Kleijne et al. [39] find that pipeline transport alone adds 1.5 $kg_{CO2\text{-}eq}/kg_{H2}$ for a distance of 1000 km and an end pressure of 80 bar. While the results of Wulf et al. [55] and Akhtar et al. [7] are comparable to our results (see Fig. 7), De Kleijne et al. [39] find that the GWI during pipeline transport is higher than our cradle-to-gate GWI including production. This large difference arises because they assume that the electricity they use for recompression has a GWI of 37 $g_{CO2\text{-}eq}$/kWh, which is more than twice as high as compared to wind electricity in our study. For liquid $H_2$ transport via trucks, Akhtar et al. [7] obtain 2.08 $kg_{CO2\text{-}eq}/kg_{H2}$

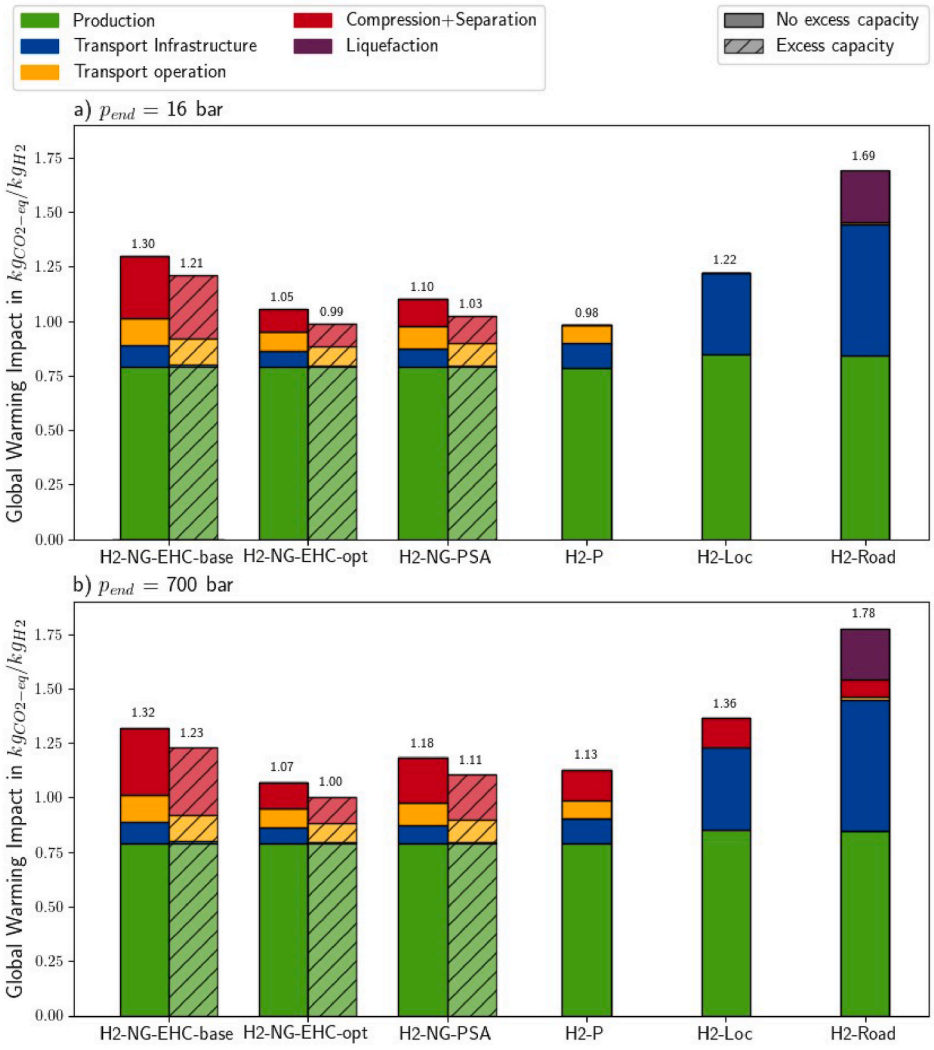



**Fig. 7.** Contribution analysis comparing the GWI of hydrogen ($H_2$) and natural gas (NG) co-transport in high-pressure distribution pipelines to the alternative $H_2$ transport routes for 20 vol.-% $H_2$ and $p_{sec}$ = 16 bar. The transport distance is 1000 km. $H_2$-NG-EHC-base and $H_2$-NG-EHC-opt are transport routes where $H_2$ is co-transported with NG and then separated via Electrochemical Hydrogen Compression (EHC). Base and opt refer to the base and optimistic case of the EHC. In $H_2$-NG-PSA, $H_2$ is co-transported with NG but subsequently separated via Pressure Swing Adsorption (PSA). $H_2$–P describes $H_2$ transport in pure $H_2$ pipelines, $H_2$-Loc describes the transport of electricity with subsequent decentral $H_2$ production at the consumer-site and $H_2$-Road describes the transport of liquid $H_2$ in fuel-cell electricic trucks. GWI: Global Warming Impact. $p_{end}$: Final pressure of the $H_2$ product, $p_{sec}$ : Operating pressure of the secondary pipeline (see Fig. 1).

for truck transport over 400 km. For $H_2$/NG co-transport with PSA, Di Lullo et al. [30] determine substantially higher values, with hydrogen separation alone adding 4.6–8.2 $kg_{CO2\text{-}eq}/kg_{H2}$. This large difference is mainly due to their use of fossil $H_2$ and carbon-intensive grid electricity, compared to green $H_2$ with wind electricity in our study. Overall, our results are comparable to the existing literature, while remaining differences are attributable to differing electricity assumptions and impact assessment methods.

Our results show that $H_2$/NG co-transport with EHC-opt maintains a lower GWI than most other transport options, including pure $H_2$ pipelines for compression up to 700 bar. Even if only separation is considered, $H_2$/NG co-transport with EHC-opt has a comparable GWI as pure hydrogen pipelines. However, wind electricity is assumed as electricity source, which leads to low electricity impacts despite high electricity demands for the separation and compression. A variation of the GWI for the electricity used in the supply chain is shown in Section 3.2.3. A contribution analysis for other volume percentages of $H_2$ in the $H_2$/NG mixture is given in Figs. S5–S7 of the SI.

### 3.2.2. Analysis of environmental burden-shift

While the green $H_2$ transport routes can reduce the GWI compared to fossil $H_2$, it is essential to assess whether these GWI reductions come at the cost of increased impacts in other environmental categories. Therefore, fossil $H_2$ serves as baseline to quantify this environmental burden-shift. All considered $H_2$ transport routes have lower impacts than the fossil reference in four to seven environmental categories (see Fig. 8). $H_2$/NG co-transport with EHC-opt or PSA and transport in pure $H_2$ pipelines reduce the environmental impacts in the categories climate change, resource depletion of energy resources ($RD_e$), ozone depletion (OD), photochemical oxidant formation (PCOF), eutrophication of terrestrial ($E_t$), acidification ($A_{tfw}$) and eutrophication marine ($E_m$) compared to the fossil reference. Among those seven environmental impact categories, $H_2$/NG co-transport with EHC-base, the local production of $H_2$ ($H_2$-Loc) and liquid $H_2$ transport via trucks ($H_2$-Road) have higher impacts than the fossil reference in $A_{tfw}$ and $E_m$, while $H_2$-Road also exceeds the impacts in $E_t$. Our results therefore show that the green $H_2$ transport routes have higher impacts than the fossil reference in at least nine out of sixteen environmental categories. Consequently, compared to the fossil reference, the environmental impacts in the

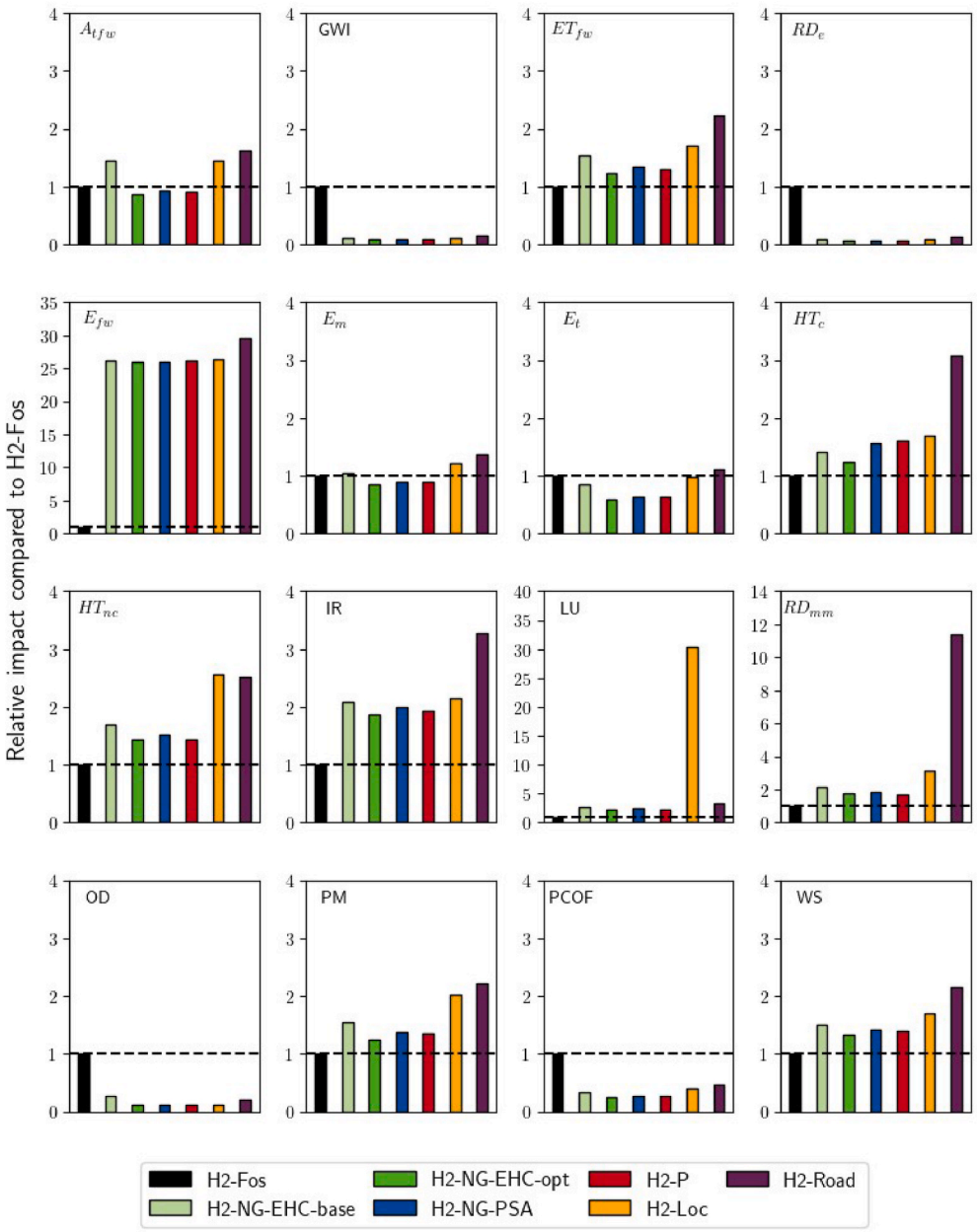



**Fig. 8.** Relative environmental impact of the green hydrogen ($H_2$) transport routes compared to the fossil reference ($H_2$-Fos) in all 16 impact categories for $p_{sec}$ = 16 bar and 20 vol.-% $H_2$. The final pressure of $H_2$ is $p_{end}$ = 700 bar. The transport distance is 1000 km. We assume that the fraction of the existing pipeline capacity used to transport $H_2$ during $H_2$/NG co-transport was previously unused and available as excess capacity (see Table 1). $p_{end}$: Final pressure of the $H_2$ product, $p_{sec}$ : Operating pressure of the secondary pipeline (see Fig. 1). $A_{tfw}$: Acidification, GWI: Global Warming Impact, $ET_{fw}$: Ecotoxicity of freshwater, $RD_e$: Resource depletion of energy resources, $E_{fw}$: Eutrophication of freshwater, $E_m$: Eutrophication of marine, $E_t$: Eutrophication of terrestrial, $HT_c$: Human toxicity carcinogenic, $HT_{nc}$: Human toxicity non-carcinogenic, IR: Ionizing radiation, LU: Land use, $RD_{mm}$: Resource depletion of metals and minerals, OD: Ozone depletion, PM: Particulate matter formation, PCOF: Photochemical oxidant formation, WS: Water use. $H_2$-NG-EHC-base and $H_2$-NG-EHC-opt are transport routes where $H_2$ is co-transported with natural gas (NG) and then separated via Electrochemical Hydrogen Compression (EHC). Base and opt refer to the base and optimistic case of the EHC. In $H_2$-NG-PSA, $H_2$ is co-transported with NG but subsequently separated via Pressure Swing Adsorption (PSA). $H_2$–P describes $H_2$ transport in pure $H_2$ pipelines, $H_2$-Loc describes the transport of electricity with subsequent decentral $H_2$ production at the consumer-site and $H_2$-Road describes the transport of liquid $H_2$ in fuel-cell electricic trucks. $H_2$-Fos is the fossil benchmark where $H_2$ is produced via Steam Methane Reforming (SMR) and transported via $H_2$ pipelines. (For interpretation of the references to colour in this figure legend, the reader is referred to the Web version of this article.)

category climate change are decreased through green $H_2$ transport routes, however, the environmental impacts in other categories are increased, so-called environmental burden-shift.

The nine impact categories, in which the green $H_2$ transport routes exceed the fossil reference are: Ecotoxicity ($ET_{fw}$), eutrophication freshwater ($E_{fw}$), human toxicity carcinogenic ($HT_c$), human toxicity non-carcinogenic ($HT_{nc}$), ionizing radiation (IR), land use (LU), resource depletion of metals and minerals ($RD_{mm}$), particulate matter formation (PM) and water use (WS). The increase in all mentioned environmental impact categories except $E_{fw}$ and WS are mainly influenced by the increased electricity demand for green compared to fossil $H_2$ production. The main driver for the increase in $E_{fw}$ and WS is the high demand of deionized water for electrolytic $H_2$ production. The high demand for deionized water also contributes to the increase in the environmental impacts of $ET_{fw}$ and IR. Besides the increased electricity demand, the material demands for the stack and BoPs of the electrolyzer and EHC

also increase the environmental impact in $RD_{mm}$ and $A_{tfw}$. For $H_2$-Loc, the construction of the transmission networks significantly increases the impacts in LU. For $H_2$-Road, the environmental impacts are the highest because of the high material requirements for vehicle production, in particular the production of liquid $H_2$ tanks.

Overall, the extent of environmental burden-shift varies among the green $H_2$ transport routes, with $H_2$/NG co-transport with EHC-opt and pure $H_2$ pipelines showing lower impacts than the fossil reference in seven out of sixteen categories. $H_2$/NG co-transport with EHC-opt achieves comparable or lower impacts than PSA in all categories, as the avoided mechanical compression reduces material and energy demands. However, our results show that the reduction of climate change impact through the employment of green $H_2$ transport routes shifts environmental burdens to other impact categories.

### 3.2.3. *Sensitivity analysis of the Global Warming Impact of the electricity source and transport distance*

In this section, the GWI of electricity supply as well as the transport distance are varied within a sensitivity analysis. In Fig. 9, the GWI of $H_2$ transport routes are shown in dependence of the GWI of electricity supply. The fossil benchmark is basically independent from electricity supply and thus shows an almost horizontal line. In contrast, the green

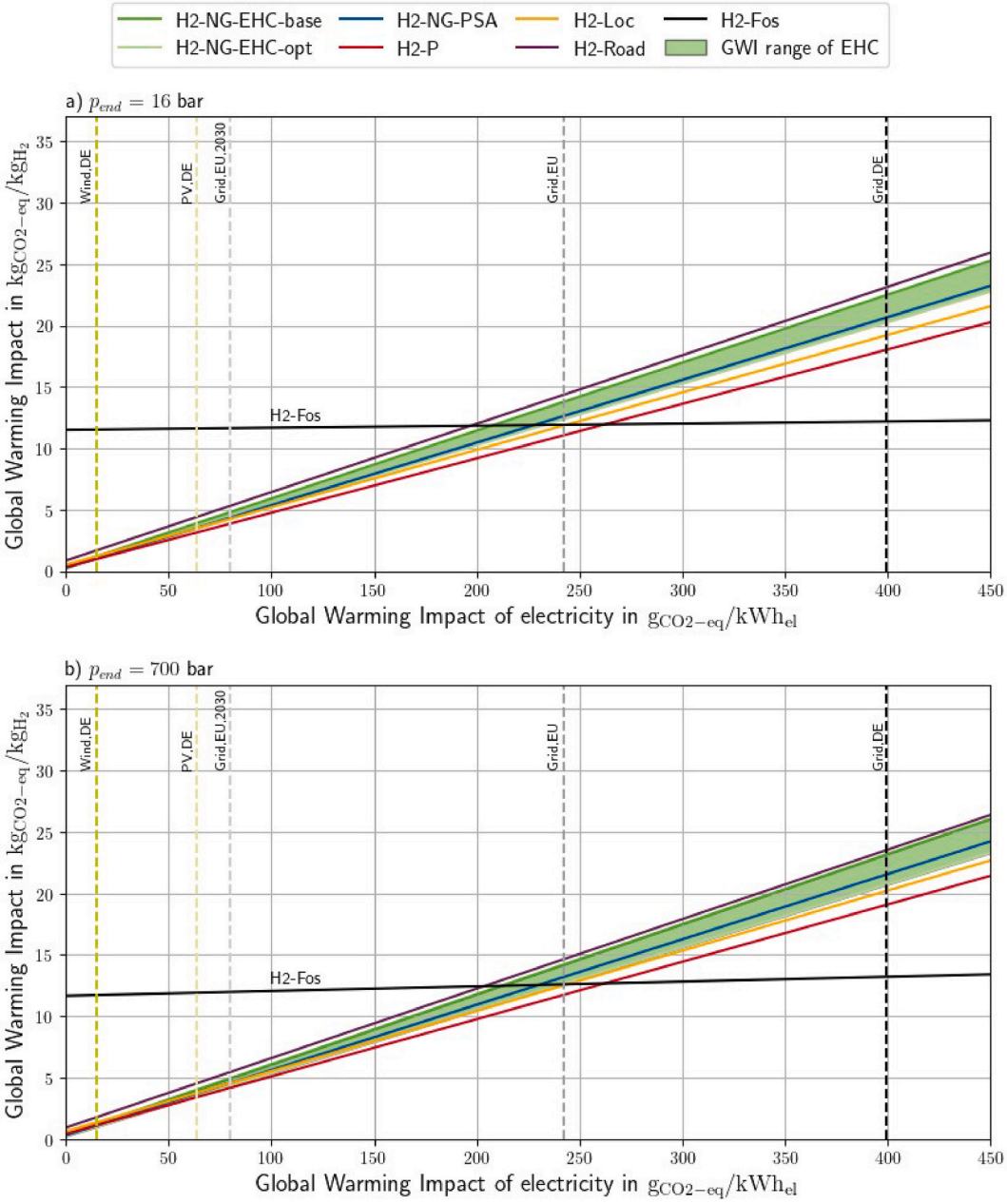



**Fig. 9.** Sensitivity analysis of the total Global Warming Impact (GWI) with respect to the GWI for the electricity source used in the $H_2$ supply chain for 20 vol.-% $H_2$ and $p_{sec}$ = 16 bar. The transport distance is 1000 km. We assume that the fraction of the existing pipeline capacity used to transport $H_2$ during $H_2$/NG co-transport was previously unused and available as excess capacity (see Table 1). $H_2$-NG-EHC-base and $H_2$-NG-EHC-opt are transport routes where $H_2$ is co-transported with natural gas (NG) and then separated via Electrochemical Hydrogen Compression (EHC). Base and opt refer to the base and optimistic case of the EHC. In $H_2$-NG-PSA, $H_2$ is co-transported with NG but subsequently separated via a Pressure Swing Adsorption (PSA). $H_2$–P describes $H_2$ transport in pure $H_2$ pipelines, $H_2$-Loc describes the transport of electricity with subsequent decentral $H_2$ production at the consumer-site and $H_2$-Road describes the transport of liquid $H_2$ in fuel-cell electricic trucks. $H_2$-Fos is the fossil benchmark where $H_2$ is produced via Steam Methane Reforming (SMR) and transported via $H_2$ pipelines. $p_{end}$: Final pressure of the $H_2$ product, $p_{sec}$ : Operating pressure of the secondary pipeline (see Fig. 1). DE: Germany, EU: Europe.

$H_2$ transport routes depend heavily on the GWI of electricity supply: the steep slopes of the green $H_2$ transport routes indicate that due to a large electricity demand within the supply chain, the GWI of electricity supply dominates the overall GWI of $H_2$ supply. Differences among the green $H_2$ transport options have a much smaller effect. The overall GWI of the green $H_2$ transport routes can even exceed that of fossil $H_2$. For example, powering the supply chain with German grid electricity would lead to GWI more than twice as high as fossil $H_2$. For most of the transport routes, even the GWI of the current European grid mix would not be sufficient to achieve a lower GWI than fossil $H_2$. However, increasing the share of renewable energy sources leads to a lower GWI than fossil $H_2$. For example, using the 2030 European grid mix (80 $g_{CO2\text{-}eq}/kwh_{el}$) results in more than 50 % reduction in GWI compared to fossil $H_2$ for all green $H_2$ transport routes. The usage of PV- or wind-electricity leads to an even higher reduction. Therefore, we emphasize that it is essential to power the entire $H_2$ supply chain with as much renewable electricity as possible.

Fig. S9 in SI shows a zoomed-in view of Fig. 9, which highlights that $H_2$/NG co-transport with EHC-opt or PSA can achieve a lower GWI than pure $H_2$ pipelines for both end pressure cases. $H_2$/NG co-transport with EHC-opt has a lower GWI than with PSA, while $H_2$/NG co-transport with EHC-base has a higher GWI than with PSA for both end pressure cases and regardless of the GWI for electricity in the supply chain.

The influence of the transport distance is shown in Fig. 10, together with a variation of the GWI of electricity. In a heat map, the most favorable transport route is identified for each combination of transport distance and GWI of electricity supply. With respect to both parameters, pure $H_2$ pipelines and $H_2$/NG co-transport with EHC-opt achieve the lowest GWI as they cover the largest areas in Fig. 10. In accordance to the results in Fig. 9, as long as the electricity has a GWI above ~260 $g_{CO2\text{-}eq}/kwh_{el}$, fossil $H_2$ has a lower GWI than all green $H_2$ transport routes.

As Fig. 10 shows, the area where $H_2$/NG co-transport with EHC-opt is preferred increases with rising transport distances and for $p_{end}$ = 700 bar. The shift in the preferred transport route with increasing transport distance is driven by the growing difference in transport impacts between pure $H_2$ pipelines and $H_2$/NG co-transport with EHC-opt (compare Section 3.2.1). For $p_{end}$ = 700 bar, pure $H_2$ pipelines require an additional compression of the $H_2$ product, which is not required for $p_{end}$ = 16 bar as the pipeline operating pressure is 16 bar. Therefore, for

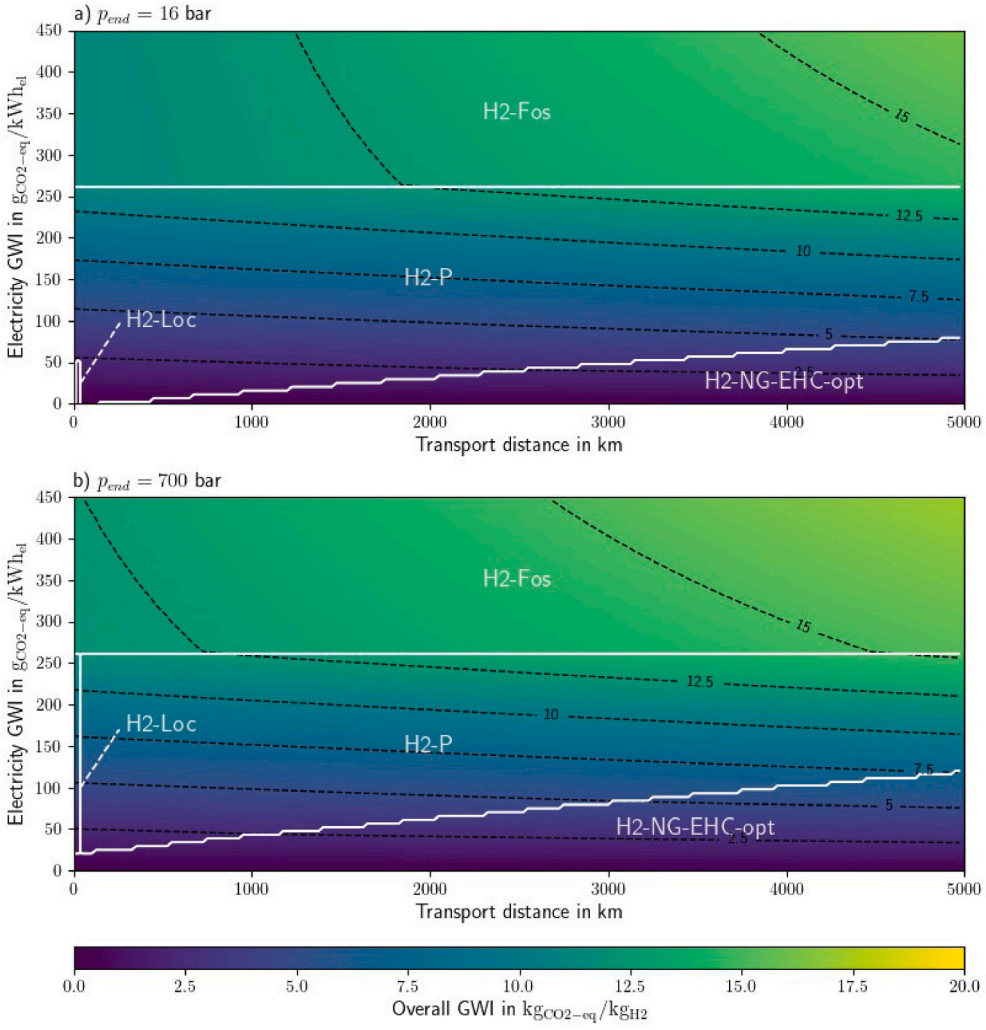



**Fig. 10.** Heat map depicting the most favorable transport route and its overall Global Warming Impact (GWI) with respect to the transport distance and the GWI for the electricity source used in the hydrogen supply chain for 20 vol.-% hydrogen and $p_{sec}$ = 16 bar. We assume that the fraction of the existing pipeline capacity used to transport $H_2$ during $H_2$/NG co-transport was previously unused and available as excess capacity (see Table 1). $p_{end}$: Final pressure of the $H_2$ product, $p_{sec}$ : Operating pressure of the secondary pipeline (see Fig. 1). $H_2$-NG-EHC-opt are transport routes where hydrogen is co-transported with natural gas (NG) and then separated via Electrochemical Hydrogen Compression (EHC). Base and opt refer to the base and optimistic case of the EHC. $H_2$–P describes hydrogen transport in pure hydrogen pipelines, $H_2$-Loc describes the transport of electricity with subsequent decentral hydrogen production at the consumer-site. $H_2$-Fos is the fossil benchmark where hydrogen is produced via Steam Methane Reforming (SMR) and transported via hydrogen pipelines. $p_{end}$: Final pressure of the hydrogen product.

$p_{end}$ = 16 bar, the lower transport impacts for $H_2$/NG co-transport with EHC-opt need to offset the additional impacts associated with separation and compression.

Figs. S15–S24 in Section 3.3 of the SI includes the heatmap in Fig. 10 for all the other cases (see Table 1). For electricity with low GWI and long transport distances, $H_2$/NG co-transport with EHC-opt is the optimal transport route in every considered case. If the unrecovered $H_2$/NG mixture of the PSA can be fed into a pipeline operating at desorption pressure of 1 bar ($p_{sec}$ = 1 bar), $H_2$/NG co-transport with PSA can also achieve the lowest GWI. If the fraction of the existing pipeline capacity used to transport $H_2$ during $H_2$/NG co-transport was previously used to transport NG (no excess capacity), the preferred area for pure $H_2$ pipelines increases as the transport impacts for the $H_2$/NG co-transport routes increase.

The sensitivity analyses allow us to make robust conclusions across all considered parameter variations: First, all green $H_2$ transport routes achieve lower GWI than fossil $H_2$ production if the GWI of electricity remains below the ~260 $g_{CO2\text{-}eq}/kwh_{el}$ threshold identified in Fig. 9, and second, $H_2$/NG co-transport with EHC consistently has a lower GWI than liquid $H_2$ transport via trucks, regardless of the considered EHC model and electricity GWI. However, the ranking between $H_2$/NG co-transport with EHC, PSA and pure $H_2$ pipelines is conditional and depends on the transport distance, end pressure, secondary pipeline pressure and the EHC model. The range between the base and optimistic EHC models can thus be interpreted as the uncertainty range in EHC performance at this stage of development.

In summary, $H_2$/NG co-transport with subsequent separation and compression via EHC has the potential to achieve similar or lower GWI as $H_2$ pipelines and $H_2$/NG co-transport with PSA, especially for long transport distances and high compression ratios, provided that the assumptions of the optimistic model need to be met.

### 3.3. Discussion

Our work assesses the environmental potential of Electrochemical Hydrogen Compression (EHC). We develop a base and optimistic model of EHC based on a 1D simulation model with several simplifications: The feed gas is assumed to consist of methane and $H_2$, neglecting other components within NG that could affect the performance of the EHC. In the optimistic case, we use literature data to model a membrane with higher conductivity leading to lower ohmic resistances. We further assume a faradaic efficiency of 100 %, which implies that neither $H_2$ back-diffusion losses nor incomplete reactions occur, even for high compression ratios. This assumption is rather optimistic and we emphasize that further research is needed to reach these conditions. In contrast, the base model accounts for these losses and represents current EHC performance, such that both models capture the uncertainty range in EHC efficiency. Nonetheless, EHC is already commercially available and high compression ratios have been shown to be reachable. For example, the Dutch startup HyET managed to develop an EHC stack, which can achieve $H_2$ pressures up to 900 bar in a single-stage compression [22].

Most important, our environmental assessment highlights that it is essential to power the green $H_2$ routes with renewable electricity. For most countries, using grid electricity with the current environmental impacts leads to a GWI higher than that of fossil $H_2$ production. This is especially relevant for $H_2$/NG co-transport with EHC since the subsequent electrochemical separation and compression causes additional energy demands compared to the other $H_2$ transport routes. Consequently, the environmental performance of EHC is particularly sensitive to the GWI of electricity supply, and the favorable results in this study rely on the use of electricity with low GWI.

While the considered green $H_2$ transport routes reduce the greenhouse gas (GHG) emissions compared to fossil $H_2$ production, the GHG emission reductions are accompanied by increased impacts in 9-11 out of 16 environmental categories. Consequently, there is an environmental burden-shift. Further investigation is required to assess the severity of the environmental burden-shift, e.g., by performing an absolute environmental sustainability assessment [75]. Although we assume wind electricity as the electricity source, the environmental burden associated with electricity use are significant due to the material demands in the wind power supply chain. For EHC specifically, the increased electricity demand as well as the material demands for the membrane and catalyst contribute to increased impacts in several categories. Besides reducing the overall electricity demand of EHC through improved energetic efficiency, the development of novel membrane materials with higher conductivity and reduced use of precious metal catalysts such as platinum are needed to reduce the environmental impacts. Improved material circularity through recycling and circular design of electrochemical components can further reduce environmental burden. Future work should include a prospective LCA of the material supply chain to account for expected changes in material production.

Our work shows that the integration of EHC into high-pressure NG distribution pipelines enables $H_2$ supply to $H_2$ consumers with low GHG emissions. Besides EHC, we consider PSA as separation unit in NG pipelines. The environmental impacts of PSA depend on which NG pipelines are available near the $H_2$ consumer. If the $H_2$ consumer is only connected to high-pressure distribution pipelines, additional energy for the PSA setup is needed to compress the unrecovered $H_2$/NG mixture. This energy demand increases for low volume percentages of $H_2$, since the amount of NG in the unrecovered $H_2$/NG mixture increases. In that case, PSA has higher environmental impacts than the optimistic model of EHC, and at 5 vol.-% $H_2$ even higher than those of the base model of EHC. If the consumer is connected to low- or mid pressure distribution pipelines, the integration of PSA leads to similar environmental impacts as the optimistic model of the EHC. Therefore, the comparison of EHC with PSA shows that EHC can achieve lower environmental impacts than PSA in most cases and offers higher design flexibility. Thus, if future development targets of the optimistic EHC model are met, it can enable $H_2$ supply via existing NG pipelines with lower environmental impacts than PSA. However, further assessment regarding economic feasibility and technical scale-up considerations is needed to fully evaluate whether EHC is more suitable for large-scale deployment.

According to the German association for gas and water (DVGW), German gas grids are ready to transport up to 20 vol.-% of $H_2$ [37]. If renewable electricity powers the entire supply chain, the co-transport of 20 vol.-% $H_2$ with subsequent separation and compression via EHC can lead to a lower GWI than transport in $H_2$ pipelines, especially for long transport distances and high compression ratios. Compared to the fossil $H_2$ production, all considered green $H_2$ transport routes can achieve a GWI reduction of at least 84 %, while $H_2$/NG co-transport with 20 vol.-% $H_2$ and subsequent separation and compression via the optimistic model of EHC can achieve a GWI reduction of up to 91 % if wind electricity is used to power the entire supply chain. Accordingly, $H_2$/NG co-transport is a promising $H_2$ transport option but should be regarded as complementary and not a substitute to pure $H_2$ pipelines. In particular, $H_2$/NG co-transport could serve as an interim solution to supply $H_2$ consumers that are not yet connected to a dedicated $H_2$ pipeline network. Within $H_2$/NG co-transport, EHC has the potential to be an essential technology for the distribution of high-purity and compressed $H_2$ using existing NG infrastructure, provided that future development targets are met.

## 4. Conclusions

We conducted a cradle-to-gate LCA to compare the environmental impacts of hydrogen ($H_2$) and natural gas (NG) co-transport in existing NG pipelines with subsequent separation and compression via EHC to other green $H_2$ transport options in 16 environmental impact categories. To capture the uncertainty range of EHC, we developed a base and optimistic case of EHC.

$H_2$/NG co-transport in existing NG pipelines with subsequent separation and compression via EHC has the potential to achieve lower

environmental impacts than transport via $H_2$ pipelines, especially for high $H_2$ end pressures and long transport distances. By relying on existing infrastructure, environmental impacts of $H_2$ transport can be reduced during $H_2$/NG co-transport. The optimistic EHC model has the potential to also achieve lower environmental impacts than Pressure Swing Adsorption (PSA), while the base model has a higher GWI than PSA, highlighting the importance of EHC efficiency improvements. All considered green $H_2$ transport routes can achieve greenhouse gas (GHG) emission reductions of at least 84 % compared to the fossil production, while $H_2$/NG co-transport with 20 vol.-% $H_2$ with EHC can reach GHG emission reductions of up to 91 % if wind power is used to power the supply chain. The GHG emissions of the electricity powering the supply chain is the dominant driver of the overall GHG emissions of green $H_2$ supply. If the GWI of the electricity exceeds ~260 $g_{CO2\text{-}eq}/kWh_{el}$, the GHG emissions of green $H_2$ supply options can even exceed those of fossil $H_2$. The deployment of green $H_2$ transport routes causes environmental burden-shift in at least 9 impact categories.

$H_2$/NG co-transport represents a promising complementary option to new pure $H_2$ pipelines. In particular, $H_2$/NG co-transport can be utilized to supply $H_2$ consumers in regions where NG infrastructure is available but no dedicated $H_2$ pipeline exists. EHC is a promising technology for large-scale $H_2$ distribution, as EHC enables the use of the extensive NG infrastructure for high-purity $H_2$ supply with low GHG emissions. However, efficiency improvements through novel membrane and catalyst materials for EHC are necessary to reach the environmental performance of the optimistic model in this work. Future work should also focus on investigating environmental burden-shift through absolute sustainability assessments and advancements of EHC by researching novel membrane and catalyst materials to improve efficiency and material circularity. As economic feasibility of EHC will ultimately drive its adoption, future work should integrate our environmental assessment with a techno-economic analysis.

## CRediT authorship contribution statement

**Karan Anand:** Writing – original draft, Visualization, Validation, Software, Methodology, Investigation, Data curation, Conceptualization. **Georgia Ioanna Prokopou:** Writing – review & editing, Conceptualization. **Wibke Zängler:** Writing – review & editing, Project administration, Conceptualization. **Vu Phong Nguyen:** Writing – review & editing, Software, Investigation, Data curation. **Hendrik Pötting:** Writing – review & editing, Visualization, Supervision, Methodology, Conceptualization. **Robert Keller:** Supervision, Project administration, Funding acquisition. **Alexander Mitsos:** Writing – review & editing, Supervision, Funding acquisition. **Matthias Wessling:** Supervision, Project administration, Funding acquisition. **Niklas von der Assen:** Writing – review & editing, Visualization, Supervision, Methodology, Funding acquisition, Conceptualization.

## Declaration of competing interest

The authors declare that they have no known competing financial interests or personal relationships that could have appeared to influence the work reported in this paper.

## Acknowledgments

This work was funded by the German Federal Ministry for Education and Research (BMBF) within the project HyInnoSep of Zukunftscluster Wasserstoff (grant number 03ZU1115CA). Support from the Deutsche Forschungsgemeinschaft (DFG) within the project IRTG 2983 Hy-Potential (ID: 516338899) is gratefully acknowledged.

## Appendix A. Supplementary data

Supplementary data to this article can be found online at https://doi.org/10.1016/j.ijhydene.2026.154957.

Abbreviations

| | |
|---|---|
| RES | Renewable electricity sources |
| $H_2$ | Hydrogen |
| NG | Natural gas |
| PSA | Pressure Swing Adsorption |
| EHC | Electrochemical Hydrogen Compression |
| SMR | Steam Methane Reforming |
| GHG | Greenhouse gas |
| GWI | Global Warming Impact |
| JRC | Joint Research Center of the European Commission |
| LCA | Life Cycle Assessment |
| FU | Functional Unit |
| $H_2$-NG-EHC-base | Hydrogen and natural gas co-transport with subsequent separation and compression via base model of EHC |
| $H_2$-NG-EHC-opt | Hydrogen and natural gas co-transport with subsequent separation and compression via optimistic model of EHC |
| $H_2$-NG-PSA | Hydrogen and natural gas co-transport with subsequent separation and compression via PSA |
| $H_2$–P | Hydrogen transport in pure hydrogen pipelines |
| $H_2$-Road | Transport of liquid hydrogen in fuel-cell electricic trucks |
| $H_2$-Loc | Transport of electricity with subsequent decentral hydrogen production at the consumer-site |
| $H_2$-Fos | Fossil benchmark where hydrogen is produced via Steam Methane Reforming (SMR) and transported via hydrogen pipelines |
| $p_{end}$ | Final pressure of the hydrogen product |
| $p_{op}$ | Operating pressure of the primary pipeline |
| $p_{sec}$ | Operating pressure of the secondary pipeline |
| PEM | Proton exchange membrane |
| LCI | Life Cycle Inventory |
| LCIA | Life Cycle Impact Assessment |
| HVAC | High-voltage alternating current |
| EF | Environmental footprint |

Mathematical symbols

| | |
|---|---|
| $x_{H2}$ | Molar fraction of hydrogen in the $H_2$/NG mixture |
| $w_{tot,EHC}$ | Total energy demand of EHC |
| $w_{el,EHC}$ | Electric energy demand of EHC |
| $w_{th,EHC}$ | Heating demand of EHC |
| $w_{cool,EHC}$ | Cooling demand of EHC |
| $m_{NG,not-Co}$ | NG mass transported in the fraction of the pipeline capacity used to transport $H_2$ in the $H_2$/NG co-transported pipeline |
| $m_{NG,Co}$ | NG mass transported with $H_2$ in the $H_2$/NG co-transported pipeline |
| $m_{H2,Co}$ | $H_2$ mass transported during $H_2$/NG co-transport |

## References


[1] Schreyer F, Ueckerdt F, Pietzcker R, Rodrigues R, Rottoli M, Madeddu S, Pehl M, Hasse R, Luderer G. Distinct roles of direct and indirect electrification in pathways to a renewables-dominated European energy system. One Earth 2024;7:226–41. https://doi.org/10.1016/j.oneear.2024.01.015.

[2] Evro S, Oni BA, Tomomewo OS. Carbon neutrality and hydrogen energy systems. Int J Hydrogen Energy 2024;78:1449–67. https://doi.org/10.1016/j.ijhydene.2024.06.407.

[3] Abdin Z, Zafaranloo A, Rafiee A, Mérida W, Lipiński W, Khalilpour KR. Hydrogen as an energy vector. Renew Sustain Energy Rev 2020;120. https://doi.org/10.1016/j.rser.2019.109620.

[4] Mio A, Barbera E, Massi Pavan A, Bertucco A, Fermeglia M. Sustainability analysis of hydrogen production processes. Int J Hydrogen Energy 2024;54:540–53. https://doi.org/10.1016/j.ijhydene.2023.06.122.

[5] Fuel cells and hydrogen 2 joint undertaking, Hydrogen roadmap Europe - a sustainable pathway for the European energy transition. 2019. https://doi.org/10.2843/249013.

[6] Korberg AD, Thellufsen JZ, Skov IR, Chang M, Paardekooper S, Lund H, Mathiesen BV. On the feasibility of direct hydrogen utilisation in a fossil-free Europe. Int J Hydrogen Energy 2023;48:2877–91. https://doi.org/10.1016/j.ijhydene.2022.10.170.

[7] Akhtar MS, Dickson R, Liu JJ. Life cycle assessment of inland green hydrogen supply chain networks with current challenges and future prospects. ACS Sustainable Chem Eng 2021;9:17152–63. https://doi.org/10.1021/acssuschemeng.1c06769.

[8] Lipiäinen S, Lipiäinen K, Ahola A, Vakkilainen E. Use of existing gas infrastructure in European hydrogen economy. Int J Hydrogen Energy 2023;48:31317–29. https://doi.org/10.1016/j.ijhydene.2023.04.283.

[9] Die Nationale Wasserstoffstrategie. Bundesministerium für Wirtschaft und Energie (BMWi) 2020. https://www.bundeswirtschaftsministerium.de/Redaktion/DE/Publikationen/Energie/die-nationale-wasserstoffstrategie.pdf?_blob=publicationFile&v=11. [Accessed 18 September 2025].

[10] Bundesministerium für Wirtschaft und Klimaschutz (BMWK). Fortschreibung der Nationalen Wasserstoffstrategie NWS; 2023. 2023, https://www.bundeswirtschaftsministerium.de/Redaktion/DE/Publikationen/Energie/fortschreibung-nationale-wasserstoffstrategie.pdf?_blob=publicationFile&v=9. [Accessed 18 September 2025].

[11] Cristello JB, Yang JM, Hugo R, Lee Y, Park SS. Feasibility analysis of blending hydrogen into natural gas networks. Int J Hydrogen Energy 2023;48:17605–29. https://doi.org/10.1016/j.ijhydene.2023.01.156.

[12] Witkowski A, Rusin A, Majkut M, Stolecka K. Analysis of compression and transport of the methane/hydrogen mixture in existing natural gas pipelines. Int J Pres Ves Pip 2018;166:24–34. https://doi.org/10.1016/j.ijpvp.2018.08.002.

[13] Department of Climate Change. Energy, the environment and water, National hydrogen strategy Australia. Barrington Stoke; 2024.

[14] Zou J, Han N, Yan J, Feng Q, Wang Y, Zhao Z, Fan J, Zeng L, Li H, Wang H. Electrochemical compression technologies for high-pressure hydrogen: current status, challenges and perspective. Electrochem Energy Rev 2020;3:690–729. https://doi.org/10.1007/s41918-020-00077-0.

[15] Prokopou GI, Faust JMM, Mitsos A, Bongartz D. Cost-optimal design and operation of hydrogen refueling stations with mechanical and electrochemical hydrogen compressors. Comput Chem Eng 2025;192:108862. https://doi.org/10.1016/j.compchemeng.2024.108862.

[16] Dehdari L, Burgers I, Xiao P, Li K Gang, Singh R, Webley PA. Purification of hydrogen from natural gas/hydrogen pipeline mixtures. Sep Purif Technol 2022;282(Part B). https://doi.org/10.1016/j.seppur.2021.120094.

[17] Nordio M, Wassie SA, Van Sint Annaland M, Pacheco Tanaka DA, Viviente Sole JL, Gallucci F. Techno-economic evaluation on a hybrid technology for low hydrogen concentration separation and purification from natural gas grid. Int J Hydrogen Energy 2021;46:23417–35. https://doi.org/10.1016/j.ijhydene.2020.05.009.

[18] Rhandi M, Trégaro M, Druart F, Deseure J, Chatenet M. Electrochemical hydrogen compression and purification versus competing technologies: part I. Pros and cons. Chin J Catal 2020;41:756–69. https://doi.org/10.1016/S1872-2067(19)63404-2.

[19] Liemberger W, Groß M, Miltner M, Harasek M. Experimental analysis of membrane and pressure swing adsorption (PSA) for the hydrogen separation from natural gas. J Clean Prod 2017;167:896–907. https://doi.org/10.1016/j.jclepro.2017.08.012.

[20] Aykut Y, Yurtcan AB. The role of the EHC system in the transition to a sustainable energy future: a review. Int J Hydrogen Energy 2023;48:23089–109. https://doi.org/10.1016/j.ijhydene.2023.03.109.

[21] Prokopou GI, Mödden ML, Mitsos A, Bongartz D. Optimal sizing and operation of electrochemical hydrogen compression. Chem Eng Sci 2024;293. https://doi.org/10.1016/j.ces.2024.120031.

[22] HyET - efficient hydrogen purification & compression. https://hyethydrogen.com/compression/. [Accessed 23 April 2025].

[23] Marciuš D, Kovač A, Firak M. Electrochemical hydrogen compressor: recent progress and challenges. Int J Hydrogen Energy 2022;47:24179–93. https://doi.org/10.1016/j.ijhydene.2022.04.134.

[24] Neacsa A, Eparu CN, Stoica DB. Hydrogen–natural gas blending in distribution systems—an energy, economic, and environmental assessment. Energies 2022;15. https://doi.org/10.3390/en15176143.

[25] Cappello V, Sun P, Elgowainy A. Blending low-carbon hydrogen with natural gas: impact on energy and life cycle emissions in natural gas pipelines. Gas Sci Eng 2024;128. https://doi.org/10.1016/j.jgsce.2024.205389.

[26] Di Lullo G, Oni AO, Kumar A. Blending blue hydrogen with natural gas for direct consumption: examining the effect of hydrogen concentration on transportation and well-to-combustion greenhouse gas emissions. Int J Hydrogen Energy 2021;46:19202–16. https://doi.org/10.1016/j.ijhydene.2021.03.062.

[27] Davis M, Okunlola A, Di Lullo G, Giwa T, Kumar A. Greenhouse gas reduction potential and cost-effectiveness of economy-wide hydrogen-natural gas blending for energy end uses. Renew Sustain Energy Rev 2023;171. https://doi.org/10.1016/j.rser.2022.112962.

[28] Bellocchi S, De Falco M, Facchino M, Manno M. Hydrogen blending in Italian natural gas grid: scenario analysis and LCA. J Clean Prod 2023;416. https://doi.org/10.1016/j.jclepro.2023.137809.

[29] Aminov RZ, Bairamov AN, Filippov SP. Comprehensive assessment of the effectiveness of the hydrogen production and transportation system. Int J Hydrogen Energy 2024;86:1358–75. https://doi.org/10.1016/j.ijhydene.2024.08.357.

[30] Di Lullo G, Giwa T, Okunlola A, Davis M, Mehedi T, Oni AO, Kumar A. Large-scale long-distance land-based hydrogen transportation systems: a comparative techno-economic and greenhouse gas emission assessment. Int J Hydrogen Energy 2022;47:35293–319. https://doi.org/10.1016/j.ijhydene.2022.08.131.

[31] Fazio S, Biganzioli F, De Laurentiis V, Zampori L, Sala S, Diaconu E. Supporting information to the characterisation factors of recommended EF Life Cycle Impact Assessment methods. European Commission; 2018. https://doi.org/10.2760/002447.

[32] DIN Deutsches Institut für Normung e. V.. Umweltmanagement – Ökobilanz – Grundsätze und Rahmenbedingungen (ISO 14040:2006 + Amd 1:2020). Deutsche Fassung EN ISO 14040:2006 + A1:2020. Berlin: Beuth Verlag GmbH; 2021.

[33] Barthélémy H. Hydrogen storage - industrial prospectives. Int J Hydrogen Energy 2012;37:17364–72. https://doi.org/10.1016/j.ijhydene.2012.04.121.

[34] Al-Sharafi A, Al-Buraiki AS, Al-Sulaiman F, Antar MA. Hydrogen refueling stations powered by hybrid PV/wind renewable energy systems: Techno-socio-economic assessment. Energy Convers Manag X 2024;22. https://doi.org/10.1016/j.ecmx.2024.100584.

[35] International Organization for Standardization (ISO). ISO 14687:2019-11 Beschaffenheit von Wasserstoff als Kraftstoff - spezifizierung des Produkts. 2019.

[36] Hertwich EG, Gibon T, Bouman EA, Arvesen A, Suh S, Heath GA, Bergesen JD, Ramirez A, Vega MI, Shi L. Integrated life-cycle assessment of electricity-supply scenarios confirms global environmental benefit of low-carbon technologies. Proc Natl Acad Sci USA 2015;112:6277–82. https://doi.org/10.1073/pnas.1312753111.

[37] Deutscher Verein des Gas- und Wasserfachs e.V. (DVGW). Größtenteils bereits H2-ready: Netze, Speicher, Komponenten. 2023. https://www.dvgw.de/medien/dvgw/leistungen/publikationen/groesstenteils-h2ready-dvgw.pdf. [Accessed 19 July 2025].

[38] Wernet G, Bauer C, Steubing B, Reinhard J, Moreno-Ruiz E, Weidema B. The ecoinvent database version 3 (part I): overview and methodology. Int J Life Cycle Assess 2016;21:1218–30. https://doi.org/10.1007/s11367-016-1087-8.

[39] de Kleijne K, Huijbregts MAJ, Knobloch F, van Zelm R, Hilbers JP, de Coninck H, Hanssen SV. Worldwide greenhouse gas emissions of green hydrogen production and transport. Nat Energy 2024. https://doi.org/10.1038/s41560-024-01563-1.

[40] Bareiß K, de la Rua C, Möckl M, Hamacher T. Life cycle assessment of hydrogen from proton exchange membrane water electrolysis in future energy systems. Appl Energy 2019;237:862–72. https://doi.org/10.1016/j.apenergy.2019.01.001.

[41] Sharma H, Mandil G, Zwolinski P, Cor E, Mugnier H, Monnier E. Integration of life cycle assessment with energy simulation software for polymer exchange membrane (PEM) electrolysis. Proced CIRP 2020:176–81. https://doi.org/10.1016/j.procir.2020.02.139. Elsevier B.V.

[42] Mehmeti A, Angelis-Dimakis A, Arampatzis G, McPhail SJ, Ulgiati S. Life cycle assessment and water footprint of hydrogen production methods: from conventional to emerging technologies. Environments - MDPI 2018;5:1–19. https://doi.org/10.3390/environments5020024.
[43] Antonini C, Treyer K, Streb A, van der Spek M, Bauer C, Mazzotti M. Hydrogen production from natural gas and biomethane with carbon capture and storage - a techno-environmental analysis. Sustain Energy Fuels 2020;4:2967–86. https://doi.org/10.1039/d0se00222d.
[44] Yin L, Ju Y. Review on the design and optimization of hydrogen liquefaction processes. Front Energy 2020;14:530–44. https://doi.org/10.1007/s11708-019-0657-4.
[45] Al Ghafri SZ, Munro S, Cardella U, Funke T, Notardonato W, Trusler JPM, Leachman J, Span R, Kamiya S, Pearce G, Swanger A, Rodriguez ED, Bajada P, Jiao F, Peng K, Siahvashi A, Johns ML, May EF. Hydrogen liquefaction: a review of the fundamental physics, engineering practice and future opportunities. Energy Environ Sci 2022;15:2690–731. https://doi.org/10.1039/d2ee00099g.
[46] Peschel A. Industrial perspective on hydrogen purification, compression, storage, and distribution. Fuel Cells 2020;20:385–93. https://doi.org/10.1002/fuce.201900235.
[47] Stolzenburg K, Mubbala R. Integrated design for demonstration of efficient liquefaction of hydrogen (IDEALHY) - hydrogen liquefaction report. 2013.
[48] Kanz O, Brüggemann F, Ding K, Bittkau K, Rau U, Reinders A. Life-cycle global warming impact of hydrogen transport through pipelines from Africa to Germany. Sustain Energy Fuels 2023;7:3014–24. https://doi.org/10.1039/d3se00281k.
[49] Tahan MR. Recent advances in hydrogen compressors for use in large-scale renewable energy integration. Int J Hydrogen Energy 2022;47:35275–92. https://doi.org/10.1016/j.ijhydene.2022.08.128.
[50] Khan MA, Young C, Mackinnon C, Layzell DB. The techno-economics of hydrogen compression. Transition Accelerator Technical Briefs 2021;1:1–36.
[51] Cebolla O, Dolci R, Dolci F. Assessment of hydrogen delivery options. Luxembourg: Publications Office of the European Union; 2022. https://doi.org/10.2760/869085.
[52] European Comission JRC, Arrigoni A, Dolci F, Ortiz Cebolla R, Weidner E, D'Agostini T, Eynard U, Santucci V, Mathieux F. Environmental life cycle assessment (LCA) comparison of hydrogen delivery options within Europe. Luxembourg: Publications Office of the European Union; 2024. https://doi.org/10.2760/5459.
[53] Télessy K, Barner L, Holz F. Repurposing natural gas pipelines for hydrogen: limits and options from a case study in Germany. Int J Hydrogen Energy 2024;80:821–31. https://doi.org/10.1016/j.ijhydene.2024.07.110.
[54] Rödl A, Wulf C, Kaltschmitt M. Assessment of selected hydrogen supply chains-factors determining the overall GHG emissions. Hydrogen Supply Chain: Design, Deployment and Operation 2018:81–109. https://doi.org/10.1016/B978-0-12-811197-0.00003-8. Elsevier.
[55] Wulf C, Reuß M, Grube T, Zapp P, Robinius M, Hake JF, Stolten D. Life Cycle Assessment of hydrogen transport and distribution options. J Clean Prod 2018;199:431–43. https://doi.org/10.1016/j.jclepro.2018.07.180.
[56] Direct current for long-distance transmission. https://medienportal.siemens-stiftung.org/de/direct-current-for-long-distance-transmission-101614. [Accessed 16 January 2025].
[57] Sacchi R, Bauer C, Cox BL. Does size matter? The influence of size, load factor, range autonomy, and application type on the life cycle assessment of current and future medium? The heavy-duty vehicles. Environ Sci Technol 2021;55:5224–35. https://doi.org/10.1021/acs.est.0c07773.
[58] Weiszflog E, Abbas M. Life cycle assessment of hydrogen storage systems for trucks. Chalmers University of Technology; 2022.
[59] Laouir A. Performance analysis of open-loop cycles for LH2 regasification. Int J Hydrogen Energy 2019;44:22425–36. https://doi.org/10.1016/j.ijhydene.2018.12.204.
[60] Mrusek S, Blasius M, Morgenroth F, Thiele S, Wasserscheid P. Hydrogen extraction from methane-hydrogen mixtures from the natural gas grid by means of electrochemical hydrogen separation and compression. Int J Hydrogen Energy 2024;50:526–38. https://doi.org/10.1016/j.ijhydene.2023.08.195.
[61] Abdulla A, Laney K, Padilla M, Sundaresan S, Benziger J. Efficiency of hydrogen recovery from reformate with a polymer electrolyte hydrogen pump. AIChE J 2011;57:1767–79. https://doi.org/10.1002/aic.12406.
[62] Yang J, Lee C-H, Chang J-W. Separation of hydrogen mixtures by a two-bed pressure swing adsorption process using zeolite 5A. Ind Eng Chem Res 1997. https://doi.org/10.1021/ie960728h.
[63] Burgers I, Dehdari L, Xiao P, Li K Gang, Goetheer E, Webley P. Techno-economic analysis of PSA separation for hydrogen/natural gas mixtures at hydrogen refuelling stations. Int J Hydrogen Energy 2022;47:36163–74. https://doi.org/10.1016/j.ijhydene.2022.08.175.
[64] Shabbani HJK, Othman MR, Al-Janabi S, Barron A, Helwani Z. H2 purification employing pressure swing adsorption process: parametric and bibliometric review. Int J Hydrogen Energy 2024;50:674–99. https://doi.org/10.1016/j.ijhydene.2023.11.069.
[65] Sircar S, Golden TC. Purification of hydrogen by pressure swing adsorption. Separ Sci Technol 2000;35:667–87. https://doi.org/10.1081/SS-100100183.
[66] Sand M, Skeie RB, Sandstad M, Krishnan S, Myhre G, Bryant H, Derwent R, Hauglustaine D, Paulot F, Prather M, Stevenson D. A multi-model assessment of the Global Warming Potential of hydrogen. Commun Earth Environ 2023;4. https://doi.org/10.1038/s43247-023-00857-8.
[67] Derwent RG, Stevenson DS, Utembe SR, Jenkin ME, Khan AH, Shallcross DE. Global modelling studies of hydrogen and its isotopomers using STOCHEM-CRI: likely radiative forcing consequences of a future hydrogen economy. Int J Hydrogen Energy 2020;45:9211–21. https://doi.org/10.1016/j.ijhydene.2020.01.125.
[68] Hauglustaine D, Paulot F, Collins W, Derwent R, Sand M, Boucher O. Climate benefit of a future hydrogen economy. Commun Earth Environ 2022;3. https://doi.org/10.1038/s43247-022-00626-z.
[69] Warwick NJ, Archibald AT, Griffiths PT, Keeble J, O'connor FM, Pyle JA, Shine KP. Atmospheric composition and climate impacts of a future hydrogen economy. Atmos Chem Phys 2023;23:13451–67. https://doi.org/10.5194/acp-23-13451-2023.
[70] Lipp L. Electrochemical hydrogen compressor. https://www.hydrogen.energy.gov/docs/hydrogenprogramlibraries/pdfs/review14/pd048_lipp_2014_o.pdf. [Accessed 4 March 2026].
[71] Jackson C, Smith G, Kucernak AR. Deblending and purification of hydrogen from natural gas mixtures using the electrochemical hydrogen pump. Int J Hydrogen Energy 2024;52:816–26. https://doi.org/10.1016/j.ijhydene.2023.05.065.
[72] Nordio M, Rizzi F, Manzolini G, Mulder M, Raymakers L, Van Sint Annaland M, Gallucci F. Experimental and modelling study of an electrochemical hydrogen compressor. Chem Eng J 2019;369:432–42. https://doi.org/10.1016/j.cej.2019.03.106.
[73] V Dale N. Characterization of PEM electrolyzer and PEM fuel cell stacks characterization of PEM electrolyzer and PEM fuel cell stacks using electrochemical impedance spectroscopy using electrochemical impedance spectroscopy. https://commons.und.edu/theses; 2009.
[74] Department of Energy U. Hydrogen fuel R&D: U.S. department of energy hydrogen and fuel cells program 2019 Annual Merit Review (AMR) and peer evaluation report. 2019.
[75] Bjorn A, Paulilo A, Sanye Mengual E, De Laurentiis V, Vea E, Hauschild MZ, Sala S. Guidance for applying absolute environmental sustainability assessment on activities at different scales (BETA version). https://doi.org/10.2760/7677803; 2025.